Molecular Therapy
Oncology
Original Article

A general pHLA-CD80 scaffold fusion protein to promote efficient antigen-specific T cell-based immunotherapy

Yue Wu,[1] Xiao Liang,[1] Yanping Sun,[1] Jiangtao Ning,[1] Yukun Dai,[1] Shijie Jin,[1] Yingchun Xu,[1] Shuqing Chen,[1,2] and Liqiang Pan[1]

[1]College of Pharmaceutical Sciences, Zhejiang University, Hangzhou 310058, China; [2]Department of Precision Medicine on Tumor Therapeutics, ZJU-Hangzhou Global Scientific and Technological Innovation Center, Hangzhou 311200, China

Inadequate antigen-specific T cells activation hampers immunotherapy due to complex antigen presentation. In addition, therapeutic *in vivo* T cell expansion is constrained by slow expansion rates and limited functionality. Herein, we introduce a model fusion protein termed antigen-presenting cell-mimic fusion protein (APC-mimic), designed to greatly mimicking the natural antigen presentation pattern of antigen-presenting cells and directly expand T cells both *in vitro* and *in vivo*. The APC-mimic comprises the cognate peptide-human leukocyte antigen (pHLA) complex and the co-stimulatory marker CD80, which are natural ligands on APCs. Following a single stimulation, APC-mimic leads to an approximately 400-fold increase in the polyclonal expansion of antigen-specific T cells compared with the untreated group *in vitro* without the requirement for specialized antigen-presenting cells. Through the combination of single-cell TCR sequencing (scTCR-seq) and single-cell RNA sequencing (scRNA-seq), we identify an approximately 600-fold monoclonal expansion clonotype among these polyclonal clonotypes. It also exhibits suitability for *in vivo* applications confirmed in the OT-1 mouse model. Furthermore, T cells expanded by APC-mimic effectively inhibits tumor growth in adoptive cell transfer (ACT) murine models. These findings pave the way for the versatile APC-mimic platform for personalized therapeutics, enabling direct expansion of polyfunctional antigen-specific T cell subsets *in vitro* and *in vivo*.

INTRODUCTION

Antigen-specific T cells play a pivotal role in initiating and regulating the immune response to antigens. The interaction of the T cell receptor (TCR) with the peptide-human leukocyte antigen (pHLA) complex (signal 1) and co-stimulatory markers such as CD80 or CD86 (signal 2) on the surface of antigen-presenting cells (APCs) is critical for the priming, activation, expansion, and subsequent destiny of antigen-specific T cells.[1] Recent advancements in immunotherapy have demonstrated that activating these specific T cells is an effective strategy for combating tumors and viruses.

Approved immune checkpoint inhibitors, including CTLA-4, PD-1, and PD-L1 antibodies,[2] have significantly improved patient outcomes.[3,4] However, their response rate is relatively low, with approximately 80% of patients showing no response.[5] In addition, they can lead to severe side effects, including cardiomyopathies, colitis, and pneumonia,[6,7] due to the activation of non-specific T cells. Adoptive cell transfer (ACT) immunotherapies include technologies such as CAR-T cell therapy,[8] which gained FDA approval in 2017 for treating CD19-positive leukemia. CAR-T therapy involves genetically modifying a patient's autologous T cells to express chimeric antigen receptor targeting CD19, enabling them to target and eliminate CD19-expressing cells.[9] Such transgenic T cells have been clinically observed to potently kill all CD19 positive cells including normal CD19 B cells. The activated CAR-T cells usually give rise to a strong cytokine storm, as a result of its non-natural mechanism of action by fusing CD3-zeta with other costimulatory domains (CD28, 4-1BB, etc.).[10] Moreover, they exhibit limited effectiveness against solid tumors.[11]

Recently, artificial antigen-presenting cells (aAPCs) have been developed to enhance control over antigen presentation[12] and activation of antigen-specific T cells. These aAPCs have various formats, including cells,[13,14] beads,[15] nanoparticles,[16,17] or scaffolds made of lipid bilayers.[18] However, they are primarily used for *ex vivo* T cell expansion instead of *in vivo* stimulation of antigen-specific T cell responses.[19] Therefore, a population of the patient's T cells are capable of targeting and killing tumor cells as long as there are sufficient antigen-specific T cells activated *in vivo*.

Herein, we describe a monovalent pHLA-CD80 scaffold fusion protein called APC-mimic, which includes the cognate pHLA complex

Received 16 January 2024; accepted 7 June 2024;
https://doi.org/10.1016/j.omton.2024.200827.

Correspondence: Shuqing Chen, College of Pharmaceutical Sciences, Zhejiang University, Hangzhou 310058, China.
E-mail: chenshuqing@zju.edu.cn
Correspondence: Liqiang Pan, College of Pharmaceutical Sciences, Zhejiang University, Hangzhou 310058, China.
E-mail: panliqiang@zju.edu.cn

and co-stimulatory marker CD80, resulting in direct antigen presentation to specific T cells and activating them in a natural way. Using epitope of human cytomegalovirus pp65 (CMV_{pp65}) and ovalbumin (OVA) as illustrative examples, we demonstrate that APC-mimic holds promise as a general immunotherapeutic agent for directing specific activation and expansion of antigen-specific T cell responses. The therapeutic potential of APC-mimic during ACT is also supported by the *in vivo* results in an immunodeficient mouse model, showing that antigen-specific T cells expanded by APC-mimic can exert killing functions *in vivo*, thereby effectively inhibiting tumor growth. The clonal expansion and transcriptome changes of expanded $CD8^+$ T cells are further characterized by the combination of single-cell TCR sequencing (scTCR-seq) and single-cell RNA sequencing (scRNA-seq). We find a significant enrichment of genes and pathways associated with T cell activation after treatment. In addition, an approximately 600-fold monoclonal expansion clonotype is identified after treatment with APC-mimic. Moreover, a murine surrogate mAPC-mimic is further tested in the tumor-bearing OT-I mouse model, which expands sufficient OVA-specific $CD8^+$ T cells directly *in vivo* and promotes tumor regression. In summary, the versatile APC-mimic platform exhibits multiple therapeutic potential by directly expanding polyfunctional antigen-specific T cell subsets, both *in vitro* and *in vivo*.

RESULTS

Design and characterization of APC-mimic

Formats of APC-mimic and its analogs are depicted in Figure 1A. APC-mimic is composed of a single IgG1 Fc, one pHLA complex, and a wild CD80 extracellular domain encoded in a two-plasmid system. Human β-2-microglobulin and MHC class I heavy chain domains α1 to α3 were shortened at the transmembrane region. The "knob-into-hole" technology can be used to create a heterodimeric structure.[20–22] To decrease Fc domain effector activity, three amino acid changes (L234A, L235A, and P329G) were added to the APC-mimic's Fc region.[23–25] To determine the preliminary effectiveness of the APC-mimic, we used the HLA-A*0201 subtype for initial proof-of-concept research on the immunostimulatory activity of the APC-mimic because it is the most prevalent MHC class I allele in the people of North America.[26] As a control, APC-mimic analogs, pHLA scaffold (which contains pHLA), and CD80 scaffold (which has CD80 but lacks pHLA domains) were expressed, and the schematic of APC-mimic for direct antigen presentation and stimulating antigen-specific $CD8^+$ T cells for cell killing is shown in Figure 1B. SDS-PAGE under reducing conditions was used to validate the analogs by visualizing the expected subunits (Figure 1C). Regarding conformational verification, both proteins still had the full ability to bind to the appropriate antibody as identified by ELISA (Figure 1D).

Peripheral blood mononuclear cells (PBMCs) from CMV-seropositive HLA-A*0201 donors that included CMV_{pp65}-specific $CD8^+$ T cells were used to determine whether APC-mimic could be employed for the activation of $CD8^+$ T cells from human T cell subpopulations. We assayed APC-mimic and pHLA scaffold for their ability to activate T cells *in vitro*. As shown in Figure 1F, they significantly increased CD69 (early marker) and CD25 (intermediate or late marker) expression in $CD8^+$ T cells than mock-treated PBMCs at different time points. Human primary T cells were cultured *in vitro,* after 2 days of treatment with different proteins, and the APC-mimic group produced a consistent larger cluster than other groups (Figure 1E).

Collectively, our results demonstrate that the pHLA component of the APC-mimic is appropriately folded and the APC-mimic can activate $CD8^+$ T cells from human T cell subpopulations.

APC-mimic selectively expands metabolism-enhanced CMV_{pp65}-specific $CD8^+$ T cells from human PBMCs without the requirement for specialized APCs

To validate the ability of APC-mimic to enrich and expand specific T cells, CMV_{pp65}-specific $CD8^+$ T cells were counted by flow cytometry after being treated with APC-mimic and its analogs at day 7 and day 14 (Figure 2A). Furthermore, treatment with APC-mimic and pHLA scaffold increased specific $CD8^+$ T cells by up to 416.2 and 71.4 times, respectively, in comparison with untreated PBMCs (Figure 2B). When CMV_{pp65}-specific $CD8^+$ T cells were grown with APC-mimic, their frequency rose from 1.1% at day 0 to 8.16% by day 7, and to 71.4% by day 14. The representative dot plots for the investigation of HLA-A*0201 CMV_{pp65} tetramer binding is shown in Figure 2C. Other donors also showed the same trend (Figure S1A). In the context of the specificity of the CMV_{pp65}-specific APC-mimic, we also employed WT1-APC-mimic as a control in an *in vitro* expansion experiment to confirm the absence of any non-specific effects attributable to the APC-mimic itself (Figure S1B). It is interesting that the final amplification frequency after being treated by APC-mimic is strongly related to the primary frequency of CMV_{pp65}-specific $CD8^+$ T cells, the fitting curve is shown in Figure 2D. After 14 days, APC-mimic, which presents pHLA (signal 1) and a costimulatory molecule (signal 2), significantly influenced the skewing of CD8 cells. Contrarily, the promotion of more evenly distributed $CD4^+$ and $CD8^+$ T cell proliferation was aided by the presentation of a single activation signal (pHLA scaffold and CD80 scaffold) (Figures 2E and 2F).

APC-mimic's impact on metabolic control was further examined using the mitochondrial dye. Cells' physiologically active mitochondria can be specifically identified using MitoTracker Red. As seen in the graph, we found that MitoTracker Red-stained $CD8^+$ T cells increased the most after APC - mimic treatment, indicating improved metabolic activity (Figure 2G).

We isolated $CD8^+$ T cells from PBMCs and cultured this population with APC-mimic to demonstrate that antigen-specific T cell proliferation in PBMCs treated with APC-mimic was not brought on by peptide presentation by PBMC-derived APCs. After a 14-day culture, antigen-specific T cell proliferation was once again seen (Figure 2H), proving that it was not the result of indigenous APCs presenting the antigen, which had a similar result to the experiments with $CD14^+$-depleted (monocyte-depleted) cells (Figure S1B).

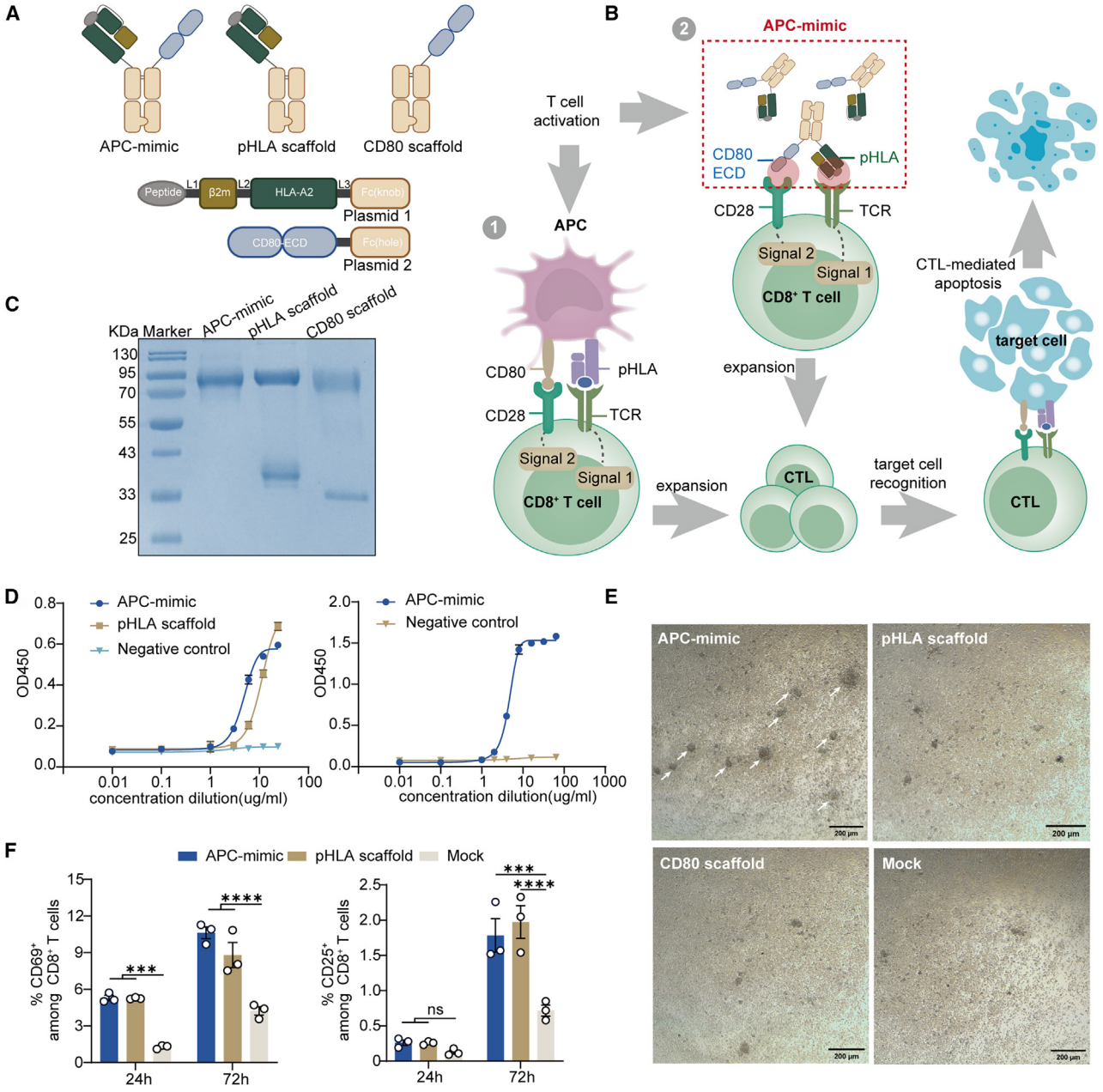

Figure 1. Design and activation capability of APC-mimic

(A) Schematic representation of the design of APC-mimic. (B) Schematic of APC-mimic for direct antigen presentation, differences in activating T cells and eliciting specific killing compared with conventional APCs. (C) SDS-PAGE gel showing the molecular weights of the reduced APC-mimic. (D) ELISA titration of APC-mimic against constant amounts of anti-HLA-ABC antibody (W6/32) (left) and anti-CD80 antibody (right). (E) Representative bright-field microscopy images of primary human T cells cultured with APC-mimic, pHLA scaffold, CD80 scaffold, or untreated (mock) for 2 days. Scale bars, 200 μm. (F) Frequencies of $CD69^+$ and $CD25^+$ subpopulation among $CD8^+$ T cells. The results are presented as means ± SEM (n = 3 independent experiments each) and were analyzed using a two-way ANOVA, followed by using Tukey's multiple comparisons test. $^{****}p \leq 0.0001$, $^{***}p \leq 0.001$, $^{**}p \leq 0.01$, $^{*}p \leq 0.05$; ns, no significance.

We also investigated two different strategies to enhance APC-mimic activity. The first strategy aimed to bolster signal 2 activation by combining the CTLA-4 antibody with the APC-mimic, resulting in a notably higher expansion ratio of antigen-specific T cells compared with using the APC-mimic alone (Figure S2A). The second strategy centered on amplifying signal 1 activation. Here, we utilized an anti-human IgG antibody to bind to the Fc segment of the APC-mimic, thereby facilitating its dimerization. Consequently, we

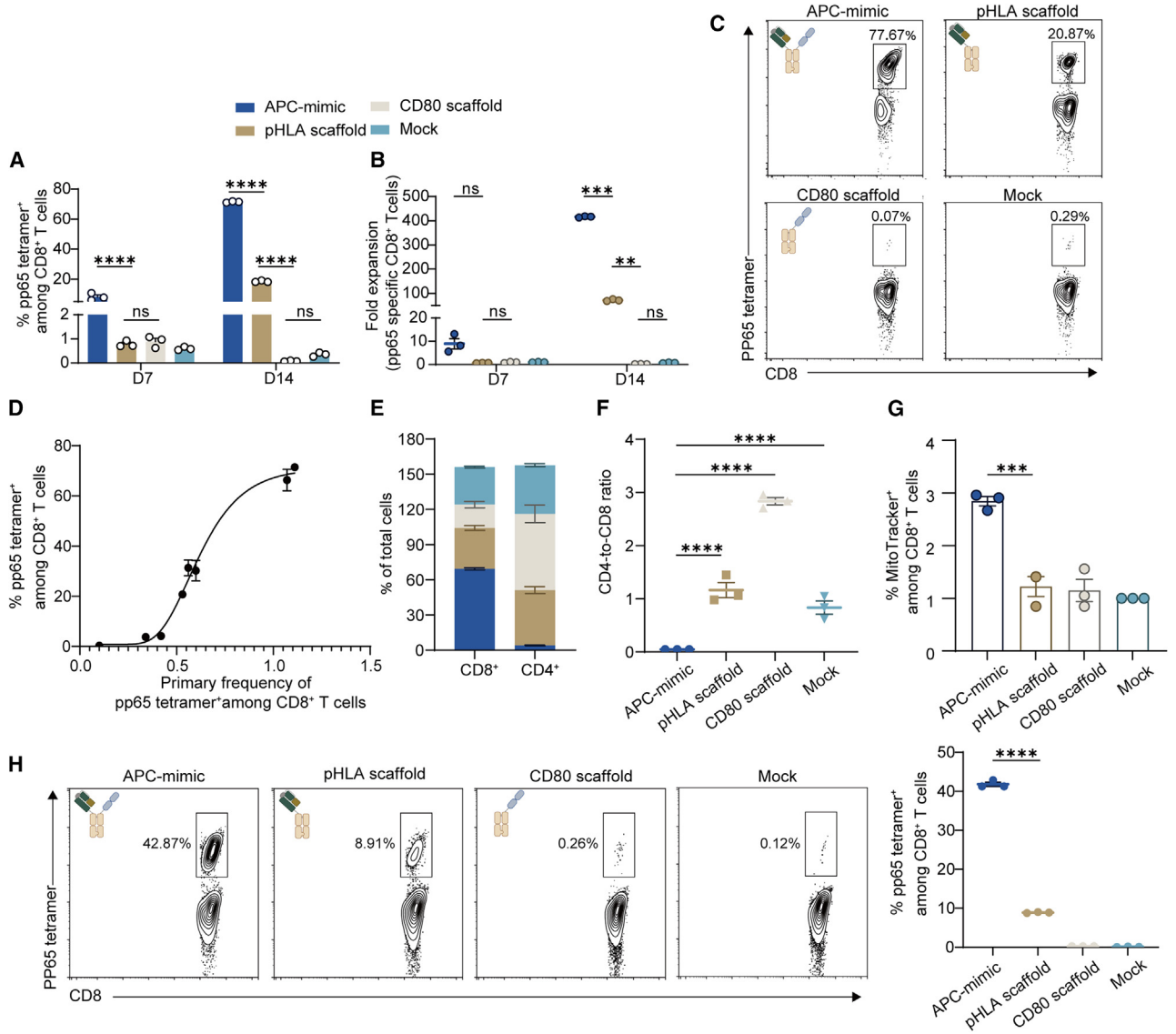

Figure 2. APC-mimic selectively expands metabolism-enhanced CMV_{pp65}-specific $CD8^+$ T cells from human PBMCs without the requirement for specialized APCs

(A) Quantification of CMV_{pp65}-specific T cells from CMV-seropositive donor T cells cultured with APC-mimic, pHLA scaffold, CD80 scaffold, or untreated (mock) on day 7 and 14. (B) Fold expansion of primary CMV_{pp65}-specific T cells cultured with APC-mimic, pHLA scaffold, CD80 scaffold, or untreated (mock). (C) Representative plot for the study of HLA-A*0201 CMV_{pp65} tetramer binding. (D) Fitting curve of the final amplification frequency after treatment with APC-mimic on day 14 and primary frequency of CMV_{pp65}-specific $CD8^+$ T cells on day 0. (E) Percentage of $CD8^+$ T cells and $CD4^+$ T cells in PBMC after treatment on day 14. (F) CD4/CD8 ratio of $CD4^+$ and $CD8^+$ single-positive cells among live $CD3^+$ cells on day 14, evaluated using FACS. (G) Percentage of MitoTracker Red staining $CD8^+$ T cells in PBMC. (H) Representative plots (left) and quantification (right) of CMV_{pp65}-specific T cells from isolated $CD8^+$ T cells that were either cultured with APC-mimic, pHLA scaffold, CD80 scaffold, or untreated (mock) on day14. The results are presented as means ± SEM (n = 3 independent experiments each) and were analyzed using a two-way ANOVA, followed by using Tukey's multiple comparisons test or one-way ANOVA and Tukey's test (E, F, and H). ****$p \leq 0.0001$, ***$p \leq 0.001$, **$p \leq 0.01$, *$p \leq 0.05$; ns, no significance.

observed an enhanced expansion of antigen-specific T cells (Figure S2B).

These findings show that APC-mimic can antigen-specifically multiply human T cells from either pure $CD8^+$ T cells or heterogeneous cell types such as PBMCs and robustly improve metabolic activity.

In vitro efficacy of APC-mimic-expanded CMV_{pp65}-specific T cells

To determine the exhaustion phenotype of $CD8^+$ T cells after being treated with APC-mimic and its analogs, we evaluated the expression of exhaustion markers and found that APC-mimic formulation resulted in a higher frequency of PD-1 and LAG-3 co-expressing

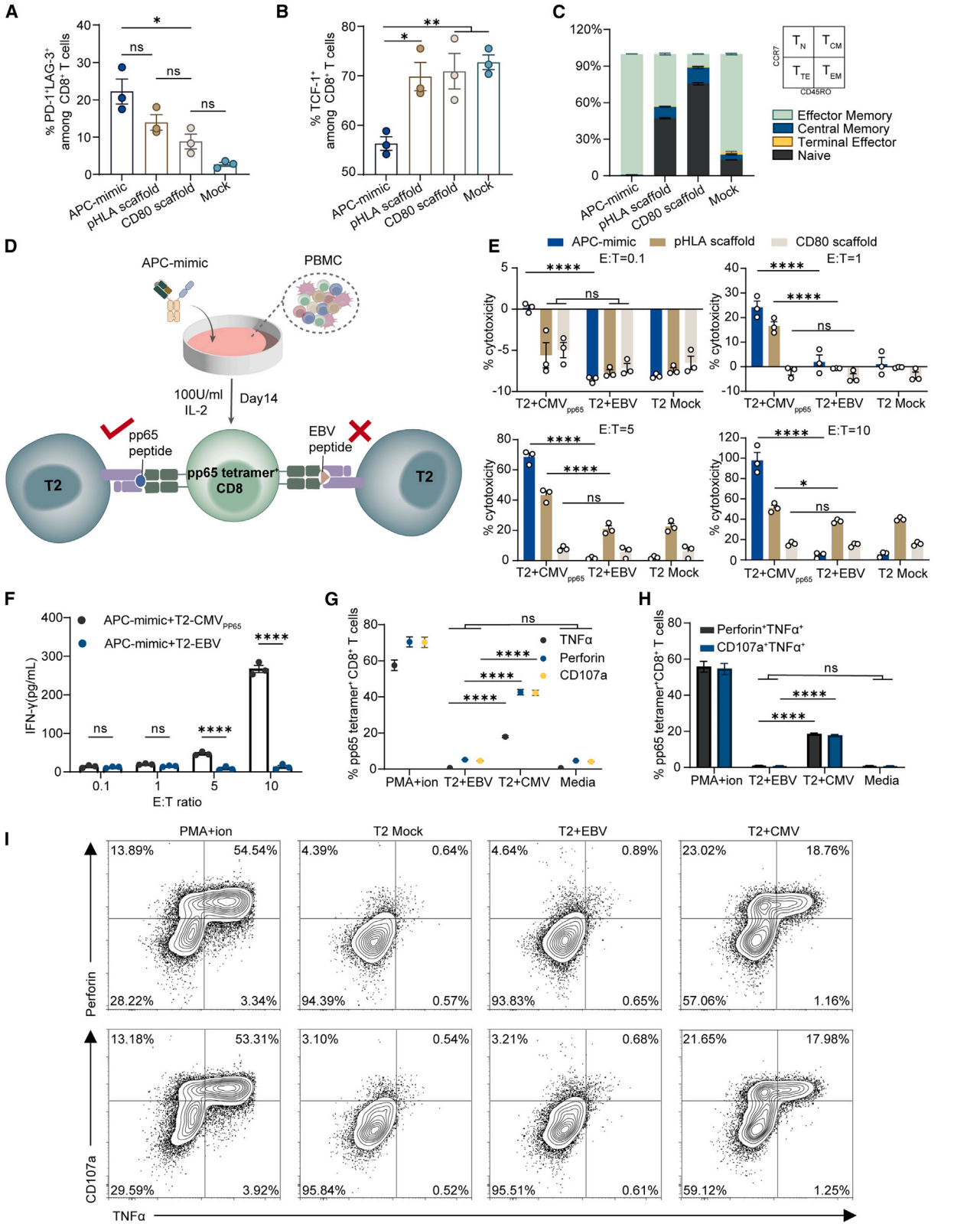

(legend on next page)

$CD8^+$ cells (Figure 3A). To delve deeper into the influence of APC-mimic on T cell activity, we delved into relevant exhaustion markers. TCF-1 serves as a marker for progenitor-exhausted T cells, while PD-1 and LAG-3 indicate terminally exhausted T cells. Our analysis unveiled that $CD8^+$ T cells expanded by the APC-mimic exhibited lower expression of TCF-1 but higher expression of PD-1 and LAG-3 compared with other groups. This indicates an enrichment of terminally exhausted T cells within the $CD8^+$ T cell population, characterized by diminished proliferative capacity but heightened killing ability, as corroborated by *in vitro* killing assays[27,28] (Figure 3B).

We also assessed the memory phenotype of the expanded CMV_{pp65}-specific $CD8^+$ T cells based on differentiating naive (T_N: $CD45RO^-CCR7^+$), central memory (T_{CM}: $CD45RO^+CCR7^+$), effector memory (T_{EM}: $CD45RO^+CCR7^-$), and terminal effector (T_{TE}: $CD45RO^-CCR7^-$) T lymphocyte subpopulations. After the enormous expansion brought on by APC-mimic treatment, CMV_{pp65}-specific T cells were significantly more likely to exhibit an effector memory ($CD45RO^+$, $CCR7^-$) phenotype (Figure 3C). These cells exhibit heightened secretion of effector molecules, such as IFN-γ and perforin, upon *in vitro* activation,[29,30] indicating their enhanced cytotoxicity and increased polyfunctionality. Therefore, it is reasonable to deduce that the APC-mimic facilitates the differentiation process of T cells into effector memory T cells, thereby enhancing their ability to exert tumor-killing activity.

Peptide-loaded T2 cells' killing assessment was designed to evaluate the polyfunctional activity of CMV_{pp65}-specific $CD8^+$ T cells activated by APC-mimic (Figure 3D). Treatment of PBMCs with APC-mimic resulted in the most potent cytotoxic activity killing of CMV_{pp65}-peptide-loaded T2 cells (stained by Calcein AM) than irrelevant EBV-loaded cells nor non-loaded cells with the increasing effector-to-target ratio, followed by pHLA scaffold and CD80 scaffold (Figure 3E), representative cell pictures taken by fluorescence microscope and mean fluorescence intensity are shown in Figure S3.

Functionality of the APC-mimic-expanded CMV_{pp65}-specific $CD8^+$ T cells was demonstrated by evaluating the generation of effector cytokines and indicators of degranulation in response to stimulation by peptide-pulsed T2 cells. IFN-γ concentration in the supernatant of co-cultures of peptide-loaded T2 cells and T cells was measured by ELISA. PBMCs expanded by APC-mimic stimulated by CMV_{pp65}-peptide-loaded T2 cells in different effector-to-target ratios were releasing more cytokines than irrelevant EBV-loaded cells (Figure 3F). When stimulated with CMV-loaded cells, more than 17% of the APC-mimic expanded tetramer-positive T cells showed a substantial increase of TNF-α, CD107a, and perforin (Figure 3G). Neither irrelevant EBV-loaded cells nor non-loaded cells resulted in the co-expression of these markers (Figure 3H), a representative dot plot is shown in Figure 3I.

These findings support that the APC-mimic promotes the differentiation of antigen-specific T cells and increases their functionality.

APC-mimic can induce $CD8^+$ T cell activation at the single-cell level and enhance their cell-killing capacity by influencing the differentiation process

We performed an extensive examination of the single-cell transcriptome and TCR profiling of T cells in the untreated or APC-mimic-treated PBMCs. Our investigation is schematized in Figure 4A. After being treated for 14 days, PBMC samples were obtained. $CD8^+$ T cells were then separated using magnetic beads, and single-cell 5′ gene-expression and V(D)J libraries were created on the 10x platform (10x Genomics, CA). A total of 8,274 T cells for the APC-mimic group and 5,389 $CD8^+$ T cells for the blank group have single-cell transcriptome data, of which 7,687 and 4,996 cells have data on both gene expression and TCR profiling.

Then we used a graph-based clustering technique implemented in Seurat[31,32] to uncover the probable functional subtypes of the total T cell population. Based on the gene expression profile, T cells were represented in 2D space using t-distributed stochastic neighbor embedding (t-SNE), and the percentage of $CD8^+$ T cell subsets in each group is shown in a bar chart (Figure 4B). We discovered 10 separate clusters that represented various cell types by evaluating the expression of traditional marker genes and their resemblance to purified bulk RNA-seq datasets.[33,34] Cell types were manually annotated, including two clusters for naive T cells, two clusters for effector memory T cells, two clusters for tissue residential T cells, and others. Furthermore, we found that APC-mimic caused changes in the composition of $CD8^+$ T cells. The proportions of effector memory T cells and exhausted T cells were significantly higher among the cell types identified in our single-cell transcriptome analysis compared with blank controls, while the proportion of naive $CD8^+$ T cells was significantly lower (Figures 4C and 4D), in agreement

Figure 3. *In vitro* efficacy of APC-mimic-expanded CMV_{pp65}-specific T cells

(A) FACS quantification of cells co-expressing PD-1 and LAG-3 among $CD8^+$ T cells in samples on the day 7 and day 14. (B) Frequencies of TCF-1^+ subpopulation among $CD8^+$ T cells. (C) Frequencies of T_N (naive, $CD45RO^-CCR7^+$), T_{CM} (central memory, $CD45RO^+CCR7^+$), T_{TE} (terminal effector, $CD45RO^-CCR7^-$) and T_{EM} (effector-memory, $CD45RO^+CCR7^-$) from CMV_{pp65}-specific $CD8^+$ T cells. (D) Schematic of CMV_{pp65}-specific $CD8^+$ T cells expanded by APC-mimic for antigen-specific cell killing *in vitro*. (E) Quantification of *in vitro* killing of mock-pulsed, EBV peptide-pulsed, or CMV_{pp65} peptide-pulsed T2 cells by CMV_{pp65}-specific $CD8^+$ T cells that were expanded for 14 days with APC-mimic, pHLA scaffold, or CD80 scaffold, and then co-cultured at various effector-to-target cell ratios, measured with a calcein-release assay. (F) Quantification of IFN-γ secretion by CMV_{pp65}-specific $CD8^+$ T cells expanded for 14 days with APC-mimic in response to co-culture at various effector-to-target cell ratios with T2 cells that were either pulsed with EBV peptide or CMV_{pp65} peptide. (G–I) Percentage of CMV_{pp65}-specific $CD8^+$ T cells upregulating TNF-α, Perforin, CD107a (G), or double-positive population (H), and representative dot plot treated as described in (I). The results are presented as means ± SEM ($n = 3$ independent experiments each) and were analyzed using a two-way ANOVA, followed by using Tukey's multiple comparisons test or one-way ANOVA and Tukey's test (A) and (B) $^{****}p \leq 0.0001$, $^{*}p \leq 0.05$; ns, no significance.

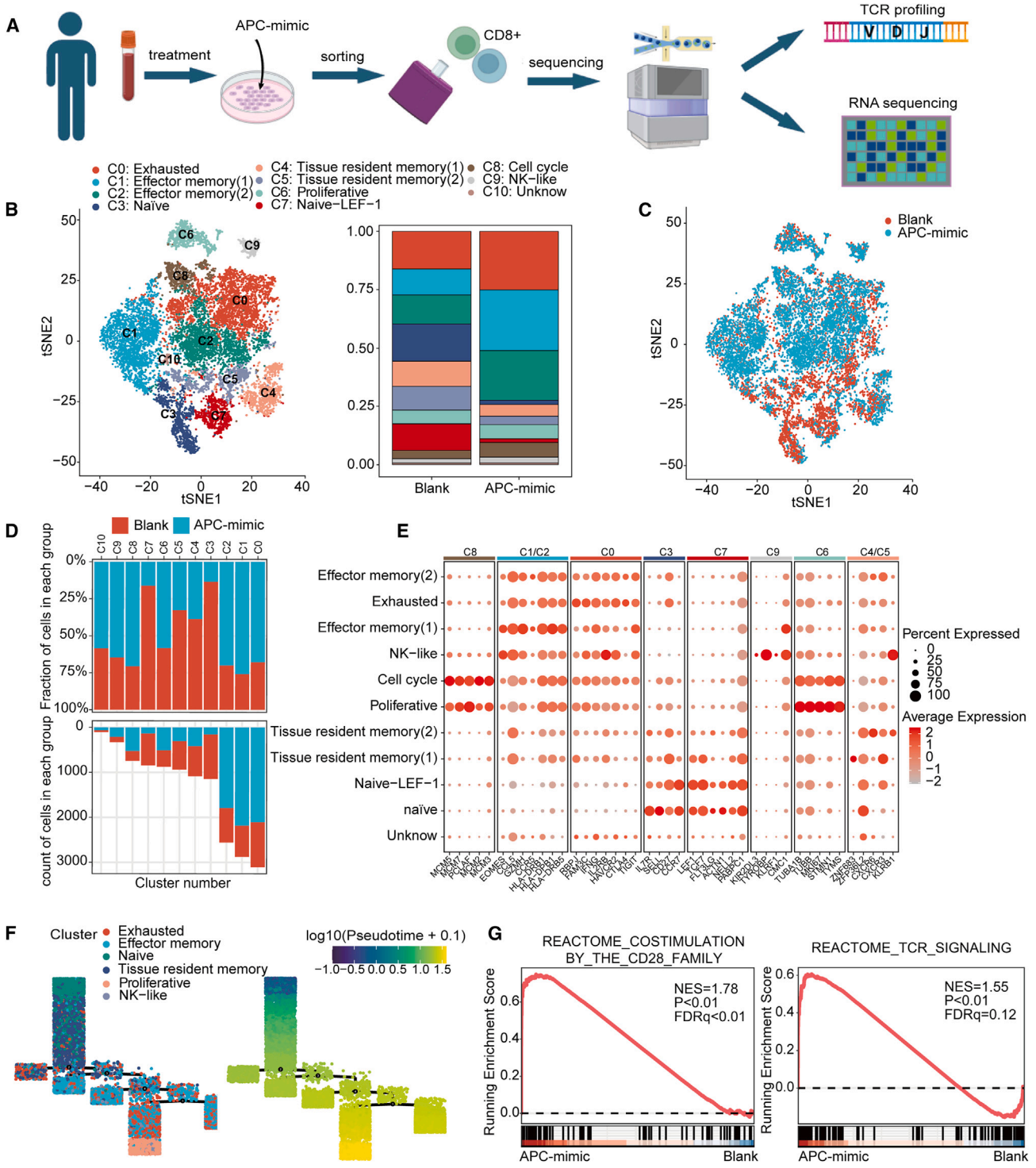

Figure 4. APC-mimic can induce CD8⁺ T cell activation at the single-cell level and enhance their cell-killing capacity by influencing the differentiation process

(A) Overview of experimental design. (B) A t-distributed stochastic neighbor embedding (t-SNE) plot of single-cell gene expression of all CD8⁺ T cells, showing 10 clusters (left), and a bar chart showing percentage of CD8⁺ T cell subsets in each group (right). Each dot corresponds to one cell and is colored according to cell cluster. (C) t-SNE plot of single-cell gene expression of CD8⁺ T cells in each group. (D) A bar chart showing fraction and counts of cells in each group between different subsets. (E) Dot plot shows

(legend continued on next page)

with the known expansion of phenotypical effector memory T cells *in vitro* experiments, which might mean that the enhancement of cell-killing capacity and cytotoxic genes were visualized in red scale on the Uniform Manifold Approximation and Projection (UMAP) subsequently (Figure S4C). Marker genes of different clusters were displayed with a dot plot (Figure 4E) and a heatmap (Figure S4A), then the highest-expressed gene of each cluster was projected onto UMAP (Figure S4B).

Using the R package Monocle 2 (version 2.14.0), we built single-cell trajectories to map the differentiation of certain cell types. Naive T cells were chosen as the beginning cell type for the differentiation. We saw a phase of transition from naive T cells to effector T cells, then proliferative T cells, which is consistent with the clustering findings (Figures 4F and S5A).

In addition, gene set enrichment analysis (GSEA) and gene set score analysis of the transcriptional variations between the APC-mimic and blank control groups showed significant enrichment of genes and pathways linked to T cell activation after treated with the APC-mimic (Figures 4G, S5B, and S5C). Then, using Gene Ontology,[35] we looked at the top differentially expressed genes in the APC-mimic group. Immune response and cell activation genes were strongly concentrated in upregulated genes of effector memory T cells (Figure S5D).

APC-mimic can facilitate monoclonal amplification

To gain a deeper understanding of clonal expansion introduced by APC-mimic, we used comparison analysis for scTCR-seq data from PBMCs treated by APC-mimic and blank control. The same clonotype was defined as cells with identical CDR3 sequences for both the TCR α and β chains.

TCRV monoclonal antibodies and CDR3 sequencing have previously been used in assessing TCR clonality.[36] We used scTCR-seq to distinguish between clonality in the APC-mimic and blank control groups. Next, we calculated the number of clonotypes occupying 11% of repositories and the percentage of clonotypes with various amplification frequencies. The most expanded TCR clones comprised up to 75% of a sequenced $CD8^+$ T cell population in the APC-mimic group, but the result was different in the blank group (Figures 5A, 5B, and S6A). For each sample, we also calculated the Shannon, Inv.Simpson, Chao, and ACE indices to assess the variety of the TCR repertoire. The APC-mimic group had considerably lower levels of this index, which positively correlates with T cell diversity, than the blank control group (Figure 5D). In addition, the aberrant CDR3 size distribution and a larger-scale power-law distribution of clone sizes also suggested that the TCR repertoire in APC-mimic was noticeably less diverse (Figure 5C). These results implied that there were clones in the APC-mimic group where significant amplification occurred.

Moreover, to identify T cells that were engaged in the immunological response, the top 5 clonotypes of all the $CD8^+$ T cells projected onto the UMAP demonstrated that, after differentiation, the percentage of $CD8^+$ T cells in the APC-mimic group steadily increased, and that these clonotypes were mostly T cells involved in the immune response (Figure 5E). To identify V and J gene fragments that differ significantly between cell types, we studied the abundance of V-J gene pair combinations in different samples and obtained specifically expressed immune genes TRAV24, TRAJ29, TRBV6-5, and TRBJ1-2, which we could use for follow-up analysis (Figures 5F and S6B).

Different sampling sites may share some of the same clonal type of cells, which also suggests that clonal migration of immune cells occurs. We tracked the top 5 clonotypes of the APC-mimic group in blank control (Figure 5G), and to visualize the network interactions of clonotypes and relationship between clonotypes across sample-cell type-grouping, we chose the most expanded clone in Figure 5G, which was an approximately 600-fold monoclonal expansion clonotype after treatment with APC-mimic (0.1299%–78.2814%) and consistent with the clonotype in Figure 5F, then, we found out that effector memory T cells and exhausted T cells share the same clonotype (Figures 5H and S5C).

Therefore, by combining scTCR-seq with scRNA-seq, transcriptome changes of $CD8^+$ T cells show a significant enrichment of genes and pathways linked to T cell activation, which is in line with design expectations. Furthermore, upregulation of cytotoxicity-related genes has the potential to contribute to tumor regression. Interestingly, we identify an approximately 600-fold monoclonal expansion clonotype after treatment with APC-mimic, suggesting that this clonotype may be essential in preventing CMV infection and that APC-mimic can facilitate monoclonal amplification.

In vivo efficacy of APC-mimic-expanded CMV_{pp65}-specific T cells

We employed a murine model to examine whether CMV_{pp65}-specific $CD8^+$ T cells expanded by APC-mimic can perform a killing function *in vivo*. In this model, K562-CMV tumor cells that had been transduced with the CMV_{pp65} antigen and validated by anti-HLA-ABC antibody (W6/32) (Figure S7A) were subcutaneously injected into NCG mice. Seven days later, the mice were treated with adoptively transferred fusion protein-expanded PBMCs (Figure 6A). The

the expression of marker genes for 10 cell clusters. The size of the dot corresponds to the percentage of cells expressing the gene in each cluster, and the color represents the average log normalized gene expression. Markers were ordered to visualize the differences between cell types. (F) Pseudo-time ordering of $CD8^+$ T cell subsets. Each dot represents a cell colored by different cell cluster (left). Darker colors in the graph represent the default starting point, lighter colors indicate further away from the pseudo-timeline starting point (right). (G) A gene set enrichment analysis (GSEA) plot of co-stimulation and TCR signaling gene set with differentially expressed genes in the APC-mimic group compared with the blank control group. GESA based on a Kolmogorov-Smirnov test.

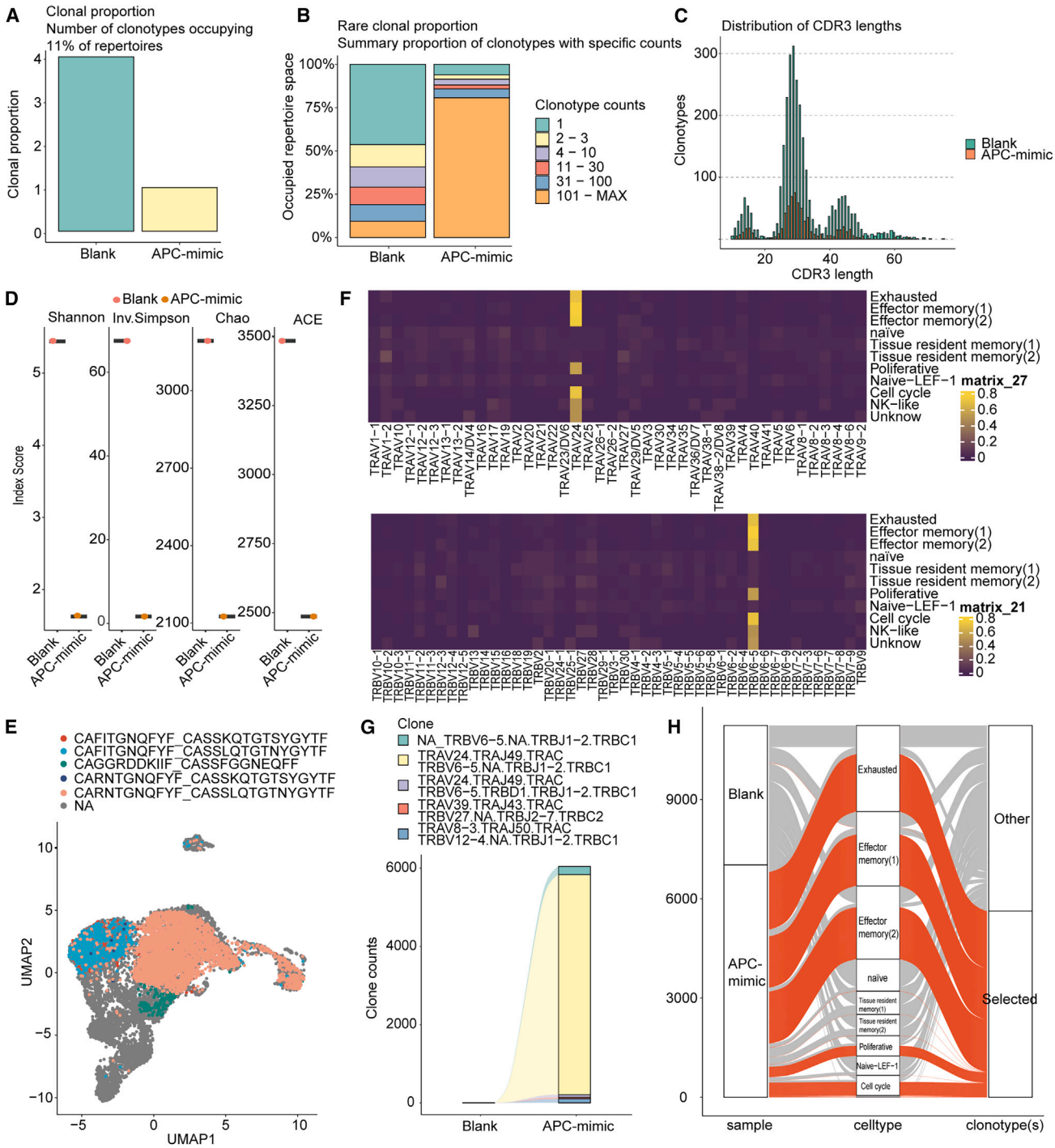

Figure 5. APC-mimic can facilitate monoclonal amplification

(A) Number of clonotypes occupying 11% of repertories. (B) Summary proportion of clonotypes with specific counts. (C) CDR3 lengths of each group were plotted, with CDR3 lengths in amino acid on the x axis and clonotypes on the y axis. (D) TCR diversity comparison between APC-mimic group and blank controls. TCR diversity was measured by Shannon, Inv.Simpson, Chao, and ACE. (E) Top 5 clonotypes of $CD8^+$ T cells were projected onto the UMAP. (F) Heatmap of V gene expression of all cell subtypes. The darker the color, the higher the expression of the V genes in that cell type. (G) The top 5 clonotype composition of APC-mimic group is represented by stacked bar plots and these clonotypes are tracked in blank control. (H) Sankey diagram of cell subset-specific clonotype tracking, with colored lines representing the distribution of top 1 clonotype in the APC-mimic group in specific types of cell subpopulations.

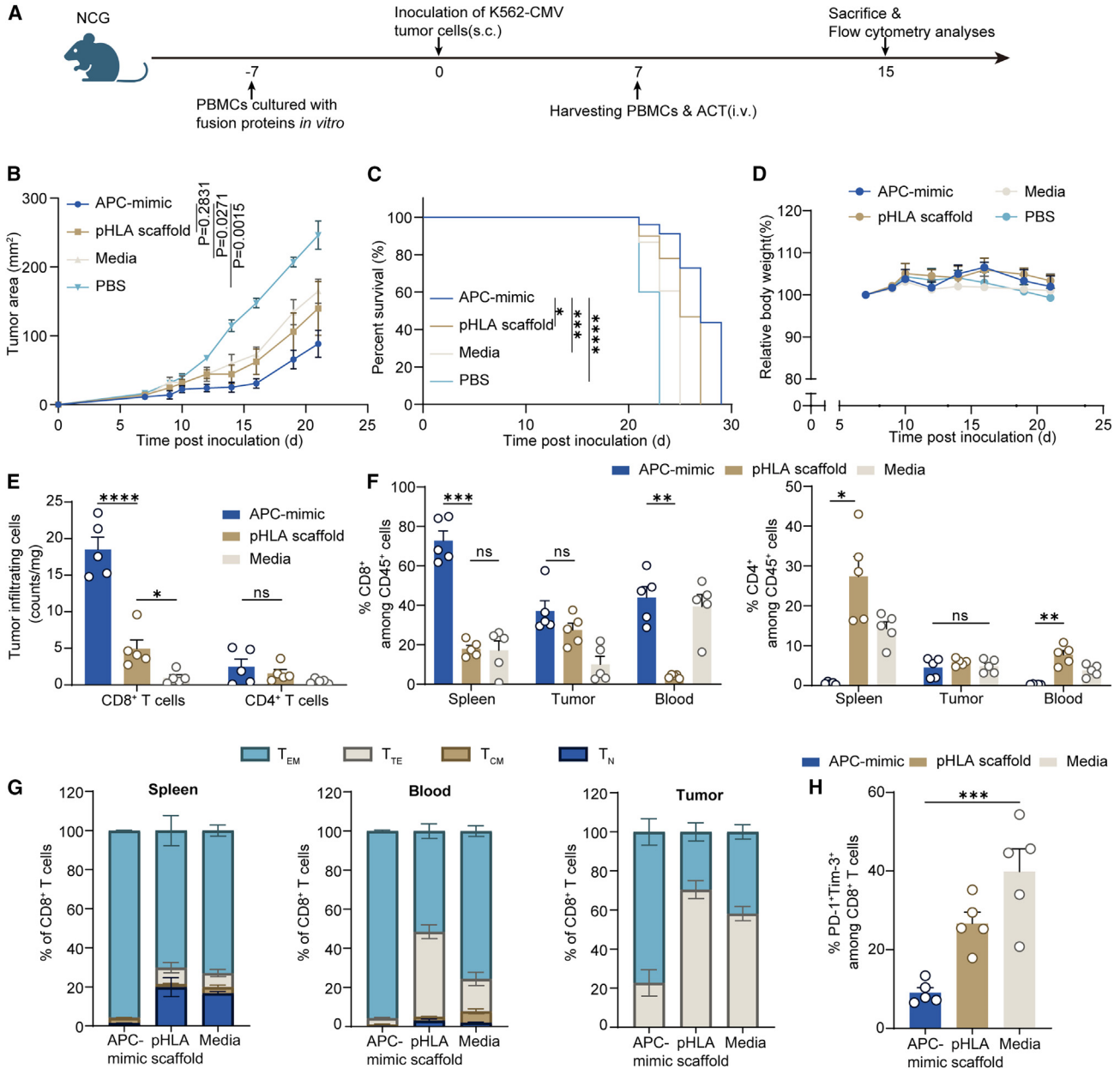

Figure 6. *In vivo* efficacy of APC-mimic-expanded CMV_{pp65}-specific T cells

(A) Study design of the adoptive cell transfer murine model. (B–D) Tumors were treated with adoptively transferred CMV_{pp65}-specific $CD8^+$ T cells that were expanded for 14 days with APC-mimic, pHLA scaffold, and untreated (medium) ($n = 4$ independent animals for PBS- and ACT-treated groups). Shown are tumor growth curves (B), survival curves (C), and relative body weight (D). (E) Counts of $CD8^+$ T cells and $CD4^+$ T cells in tumor infiltrating cells ($n = 5$ independent animals). (F) Percentage of $CD8^+$ T cells and $CD4^+$ T cells in tumor, spleen, and blood ($n = 5$ independent animals). (G) Frequencies of T_N (naive, $CD45RO^-CCR7^+$), T_{CM} (central memory, $CD45RO^+CCR7^+$), T_{TE} (terminal effector, $CD45RO^-CCR7^-$), and T_{EM} (effector-memory, $CD45RO^+CCR7^-$) from $CD8^+$ T cells in tumor, spleen, and blood ($n = 5$ independent animals). (H) Frequencies of PD-1^+TIM-3^+ subpopulation among $CD8^+$ TILs treated as described in (A)–(C) ($n = 4$ independent animals). The results are presented as means ± SEM and were analyzed by two-sided Student's t test for tumor growth data and log rank test for survival curves or one-way ANOVA and Tukey's test (D and H) or two-way ANOVA, followed by using Tukey's multiple comparisons test (E–G). $^{****}p \leq 0.0001$, $^{***}p \leq 0.001$, $^{**}p \leq 0.01$, $^{*}p \leq 0.05$; ns, no significance.

function of CMV_{pp65}-specific $CD8^+$ T cells in these four groups could be directly compared, since on the day of therapy, all of the cells were culturing and operating in the same way. Overall, culturing with APC-mimic dramatically increased the anti-virus immunity mediated by antigen-specific CTLs, as seen by decreased tumor volume and improved survival compared with both non-treated and pHLA

scaffold-expanded PBMCs (Figures 6B and 6C). Furthermore, adoptive treated T cell transferring was safe and exhibited no overt toxicities. None of the treated animals lost body weight (Figure 6D) or had their serum levels of biochemical indicators rise (Figure S7C). On day 7 after adoptive transfer of APC-mimic-expanded PBMCs, we detected a higher absolute number of $CD8^+$ T cells in tumor infiltration cells (Figure 6E), and a higher percentage of $CD8^+$ as well as a lower percentage of $CD4^+$ T cells in tumor, spleen, and blood (Figure 6F), and the CD4-to-CD8 ratio performed the same trend with *in vitro* experiment (Figure S7B). At the same time, there were fewer PD-1 and Tim-3 co-expressing $CD8^+$ T cells in comparison with non-treated and pHLA scaffold-expanded PBMCs in the tumor (Figure 6H). In addition, tumor, spleen, and blood APC-mimic-activated PBMCs were able to retain a larger proportion of original effector memory T cells (Figure 6G).

As a result, the murine model supports that CMV_{pp65}-specific $CD8^+$ T cells expanded by APC-mimic can perform a killing function *in vivo* through the treatment with adoptively transferred T cells.

Murine surrogate of APC-mimic amplifies functional OVA-specific $CD8^+$ T cells in OT-I mice to promote tumor regression

To evaluate APC-mimic's activity in a murine model, a murine surrogate of APC-mimic (mAPC-mimic) with functionally similar domains was created. The H-2Kb-$OVA_{257-264}$peptide-MHC complex, the mouse CD80 domain, and the effector-attenuated murine IgG2a Fc are all present in mAPC-mimic. We used OT-I spleen cells, a TCR transgenic population that expresses a receptor that recognizes OVA peptide coupled to H-2Kb, to evaluate the effects of mAPC-mimic on antigen-specific T cells. We next evaluated the *in vitro* functional activity of mAPC-mimic by inducing effector molecule expression in OT-I spleen cells following co-incubation with B16F10-OVA tumor cells (presenting OVA antigen). The cytokines released by mAPC-mimic-expanded OT-I cells were all detected using flow cytometry, while the minimal cytokine production induced by naive OT-I spleen cells was observed (Figure 7A).

The OT-I mouse model was used to test the *in vivo* activity of mAPC-mimic. Weekly intravenous treatment of OT-I mice with a different dose of mAPC-mimic was done twice (Figure 7B), then effector T cell activation was determined by antigen-specific TNF-α and IFN-γ production after *ex vivo* peptide stimulation for 24 h through flow cytometry analysis (Figure 7C), and IFN-γ was additionally detected locally with ELISpot. Representative IFN-γ positive spots at each dose are shown in Figures 7D and 7E. To determine the direct contribution of mAPC-mimic in tumor growth control, we transferred OT-I spleen T cells to mice bearing B16F10-OVA tumors (Figure 7F). The combination therapy of ACT and mAPC-mimic-treatment induced slower tumor outgrowth, implying that the OVA-specific $CD8^+$ T cells responded directly to mAPC-mimic for enhanced anti-tumor efficacy (Figure 7G).

Therefore, these results demonstrate that an OVA-specific population can be expanded from an existing T cell population by simply injecting mAPC-mimic intravenously *in vivo* and have characteristics of CTLs that can promote tumor regression.

DISCUSSION

The majority of immune-based treatments require the activation of antigen-specific T cell subsets, but manipulation of the antigen presentation process to activate them can be very difficult, requiring complex strategies that are challenging to translate. In addition, therapeutic *in vivo* T cell expansion is constrained by limited functionality. In this paper, we describe the activity and function of the APC-mimic fusion protein, which mimics the natural presentation of antigen-presenting cells, resulting in robust stimulation, activation, expansion, and differentiation of specific $CD8^+$ T cells both *in vitro* and *in vivo*. It also paves the way for the versatile APC-mimic platform to develop various immunotherapy strategies.

It is imperative to exercise caution in the structural design of T cell-activating proteins. Consequently, the APC-mimic fusion protein incorporates the cognate pHLA complex and the co-stimulatory marker CD80, which are natural ligands on APCs. This design ensures the selective delivery of peptide-specific TCR activation and costimulatory signals. An important safety consideration is the potential for unwanted TCR crosslinking, which can activate T cells in the absence of target cells.[37] To reduce this risk, APC-mimic exclusively features a monovalent pHLA molecule that interacts with a single TCR on a CD8 T cell.[38]

Regarding the choice of the costimulatory molecule, we chose CD80, a natural ligand for CD28, as an integral part of the APC-mimic protein. This selection diverges from the use of CD28 monoclonal antibodies, which can induce systemic inflammatory response syndrome in the absence of contaminating pathogens, endotoxin, or underlying diseases, as exemplified by TGN1412, a CD28 superagonist.[39] To enhance safety in first-in-human clinical testing using monoclonal antibodies, several measures have been proposed.[40] Although CD80 is a shared ligand for CTLA-4 and CD28,[41,42] studies by Sugiura et al.[43] and Zhao et al.[44] demonstrate that CD80 engages in a *cis*-directional interaction with PD-L1 on APCs, disrupting the PD-L1/PD-1 binding, therefore, PD-L1 is unable to prevent T cell activation when APCs exhibit high levels of CD80. The result supports our observation that APC-mimic predominantly promotes T cell activation rather than inhibition.

We performed single-cell sequencing on the expanded $CD8^+$ T cells to investigate the regulatory effects of APC-mimic on signal transduction and its impact on T cell clonal phenotypes. This analysis revealed the emergence of a novel T cell clonotype that exhibited a substantial increase in numbers following APC-mimic treatment. Intriguingly, this clonotype was found within the repertoires of functional T cell subsets, including T_{EM} and T_{EX}, which aligns with the findings of Miyama et al.[45] Although cohort size and sample depth can influence the frequency and the number of shared TCRs,[46] the increased frequency of shared clonotypes and the presence of markedly similar

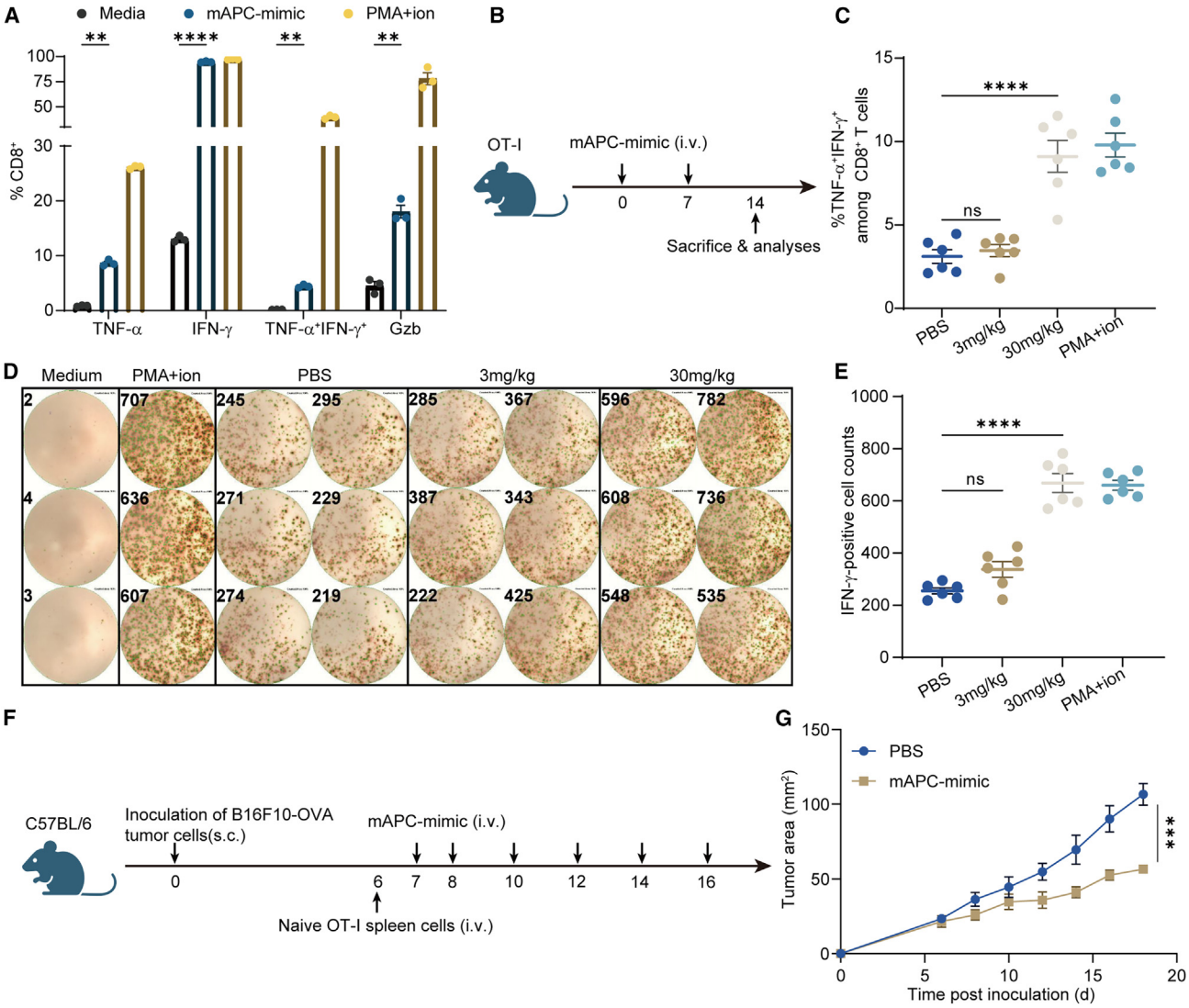

Figure 7. Murine surrogate of APC-mimic amplifies functional OVA-specific CD8⁺ T cells in OT-I mice to promote tumor regression

(A) Quantification of cytokines TNF-α, IFN-γ, and GrB secreted by OVA-specific CD8⁺ T cells expanded for 14 days with mAPC-mimic and in response to co-culture with B16F10-OVA cells as measured by flow cytometry. (B) Experimental timeline (n = 6 independent animals). (C) Frequencies of TNF-α and IFN-γ double-positive CD8⁺ T cells that were followed by *ex vivo* peptide stimulation for 24 h. (D and E) IFN-γ-positive cells among OT-I spleen cells treated as described in (B), after stimulation, the number of IFN-γ-positive cells was enumerated by ELISpot: IFN-γ-positive cell counts (E), representative images of IFN-γ ELISpot wells, the tan dots are IFN-γ-positive cells and the number in the upper left of each well represents the number of positive cells (D). (F) Experimental timeline (n = 4 independent animals). (G) Tumor growth curves. The results are presented as means ± SEM and were analyzed using a two-way ANOVA, followed by using Tukey's multiple comparisons test (A), or one-way ANOVA and Tukey's test (C and E), or two-sided Student's t test (G). ****$p \leq 0.0001$, **$p \leq 0.01$.

CDR3 sequences suggest that this shared TCR may play a significant role. Our findings indicated that this specific TCR was reactivated following exposure to APC-mimic, suggesting its crucial role in preventing CMV infection.

Despite the fact that APC-mimic primarily targets CMV_{pp65}-specific T cells, it is essential to consider the initial percentage of specific T cells that are present (as depicted in Figure 2G). Concerning signal 1, it is known that T cells exhibit natural cross-reactivity.[47] Therefore, when previously undiscovered pHLA complexes emerge, such as those in cells infected by a virus or undergoing somatic mutations, the selected T cells may possess sufficient affinity for these emerging pHLA complexes to trigger an appropriate response.[48] For the signal 2, it's notable that CD80 demonstrates a higher monomeric affinity for CTLA-4 than CD28 (CD80-CD28 ~4 μM and CD80-CTLA-4 ~0.2 μM).[42] As such, there is a reasonable assumption that enhancing the affinity of the pHLA complex and CD80 for CD28 could potentially enhance the effectiveness of APC-mimic. This enhancement

may open the possibility of activating rare specific T cells, such as tumor neoantigen-specific T cells.[49]

A versatile APC-mimic platform may be helpful in developing various immunotherapy strategies by expanding polyfunctional antigen-specific T cell subsets directly *in vivo*. In the field of tumor immunotherapy, while vaccination can induce clonal expansion of neoantigen-specific T cells, its direct anti-tumor efficacy has only been demonstrated in a limited number of patients.[50,51] Hence, combination therapies, such as a tunable molecular that can be used *in vivo* such as APC-mimic fusion protein, which can amplify the effects of neoantigen therapeutic vaccines by promoting the *in vivo* expansion of neoantigen-specific T cells, come into play in this situation.

In conclusion, we devised a general pHLA-CD80 scaffold fusion protein that manipulates the antigen presentation process in a natural manner. Our findings demonstrate that it facilitates direct stimulation, resulting in an approximately 400-fold increase in polyclonal expansion and an approximately 600-fold increase in monoclonal expansion of antigen-specific T cells. Furthermore, by substituting the pHLA complex, it can be applied in the realms of antiviral and tumor immunotherapy, demonstrating its safety. Therefore, this fusion protein paves the way for the versatile APC-mimic platform to develop various immunotherapy strategies, enabling direct expansion of polyfunctional antigen-specific T cell subsets both *in vitro* and *in vivo*.

MATERIALS AND METHODS

Mice

The Public Health Service Policy on Human Care and Use of Laboratory Animals served as a guide for conducting animal research. Zhejiang University's Committee for Ethics of Animal Experiments gave its approval for this project. Female immune-deficient strain NCG (NOD/ShiLtJGpt-Prkdc^{em26Cd52}Il2rg^{em26Cd22}/Gpt) mice aged 6–8 weeks obtained from GemPharmatech (Jiangsu, China). C57BL/6 mice and TCR-transgenic OT-I mice (C57BL/6-Tg (TcraTcrb)1100Mjb/J) were originally purchased from The Jackson Laboratory and maintained in the Laboratory Animal Center of Hangzhou Medical College. The mice were housed at the Laboratory Animal Center for at least a week before enrollment in the study under standard settings of 20°C–26°C and 40%–70% relative humidity.

Cell lines and cell culture

The Comprehensive AIDS Research Center (Tsinghua University) graciously donated human embryonic kidney 293 F cells (HEK293F), which were rotationally grown in SMM 293-TI medium (Sino Biological) supplemented with 0.5% fetal bovine serum (FBS) (Gibco). Human erythroleukemic cell line K562 was purchased from the American Type Culture Collection (ATCC) and maintained in RPMI 1640 (Gibco) with 10% FBS. B16F10-OVA were purchased from ATCC and maintained in DMEM (Gibco) with 10% FBS. The TAP-deficient T2 cell line was maintained in IMDM (Gibco) with 15% FBS. Human PBMCs were purchased from SAILYBIO (200174) and rested for 4–12 h in ImmunoCult-XF T Cell Expansion Media (STEMCELL Technologies) with 10% FBS before use. All cells were kept alive in a medium supplemented with 1% penicillin-streptomycin at 37°C, 5% CO_2, and 95% humidity, for several experiments, $CD8^+$ T cells were extracted from PBMCs using immunomagnetic sorting (STEMCELL Technologies) with human CD8 microbeads and a cocktail of antibodies to exclude non-$CD8^+$ T cells. CD14-depleted PBMCs were obtained following an additional $CD14^+$ cell isolation using MOFLO XDP.

Expression and purification of proteins

HEK293F cells were transiently co-transfected with plasmids expressing the relevant chains to produce fusion proteins.[38,52] To find the ideal DNA ratios for large-scale expression, plasmids were titrated in small-scale co-transfection experiments. On the day of transfection, plasmid DNA (sterilized through a 0.22 m PES filter [Corning]) and poly-ethyleneimine (PEI) (Polysciences) were separately diluted to 0.05 and 0.1 mg/mL in SMM 293-TII Expression Medium (serum-free, with glutamine, complete medium) (Sinobiological), then PEI, and diluted DNA were combined in equal quantities and given a further 15 min of incubation at 20°C. Subsequently, The DNA/PEI mixture (20 mL/L cells) was added to the flask along with the HEK293F cells, which was then incubated at 37°C with shaking for 3–5 days. HEK293F supernatants were used to collect secreted protein, which was then purified using HiTrap Protein A HP affinity chromatography and size-exclusion chromatography on an AKTA pure 25 device with a Superdex 200 column (Cytiva). PBS was used to store all proteins. SDS-PAGE analysis was used to confirm purity.

ELISA-based binding assays

We employed 96-well enzyme-linked immunosorbent assay (ELISA)/radioimmunoassay plates provided by Corning for the immobilization of the fusion protein and subsequent analysis of antibody-antigen interactions.[53,54] Subsequently, biotinylated antibodies were introduced at progressively decreasing concentrations. To facilitate detection, we utilized horseradish peroxidase-labeled streptavidin supplied by Beyotime. To conclude the assay, a stop solution was added to each well, and the optical density was measured at 450 nm using a microplate reader.

Antibodies

Biotin anti-human CD80 antibody (BioLegend, 305204) and biotin HLA-ABC antibody (Thermo Fisher, 13-9983-82) were used to determine the structure of the fusion proteins. BV421 mouse anti-human CD4 (BD, 562424), PE-Cy7 mouse anti-human CD8 (BD, 557746), Clear Back (human Fc receptor blocking reagent) (MBL, MTG-001), and T-Select HLA-A*02:01 CMV pp65 tetramer-NLVPMVATV-PE (MBL, TS-0010-1C) were used to identify tetramer-stained $CD8^+$ T cells using flow cytometry. APC mouse anti-human CD69 (BD, 555533) and PE mouse anti-human CD25 (BD, 555432) were utilized to confirm the fusion protein's role in activating T cells. FITC mouse anti-human CD14 (BD, 555397) was utilized to separate $CD14^+$ monocytes from PBMCs. For phenotype marker expression, FITC anti-human CD3 antibody (BioLegend,

300406), brilliant violet 605 anti-human CD107a (LAMP-1) antibody (BioLegend, 328633), APC anti-human CD279 (PD-1) antibody (BioLegend, 329907), brilliant violet 605 anti-human CD223 (LAG-3) antibody (BioLegend, 369323), FITC anti-human CD366 (Tim-3) antibody (BioLegend, 345021), FITC anti-human CD197 (CCR7) antibody (BioLegend, 353215), and Pacific blue anti-human CD45RO antibody (BioLegend, 304215) were used. For intracellular cytokine staining, FITC mouse anti-human TNF-α (BD, 562082), Alexa Fluor 647 anti-human perforin antibody (BioLegend, 308109), PE/Cyanine7 anti-mouse IFN-γ antibody (BioLegend, 505825), APC anti-mouse TNF-α antibody (BioLegend, 506307), eFluor 450 CD8a monoclonal antibody (Thermo Fisher, 48-0081-82), and FITC anti-human/mouse granzyme B antibody (BioLegend, 515403) were used.

In vitro antigen-specific T cell expansion studies

PBMCs from healthy human donors were purchased as frozen stocks (SAILYBIO). Before culture, donor samples underwent FACS analysis to check for HLA-A*0201 expression and serum exposure to CMV in the past. For expansion investigations, only HLA-A2 and CMV-experienced donors were employed. These samples were also examined for baseline CMV_{PP65}-specific $CD8^+$ T cell frequencies. In 48-well microtiter plates with ImmunoCult-XF T Cell Expansion Media (STEMCELL Technologies), 2×10^5 PBMCs, $CD8^+$ T cells, or $CD14^+$ monocyte-depleted PBMCs were stimulated with fusion proteins. In expansion studies, mock-treated samples were grown in a T cell medium devoid of fusion proteins. Recombinant human IL-2 from PeproTech (100 U/mL) was introduced on day 2. Half-medium changes and IL-2 supplementation were carried out every other day beginning on day 5. The cells were taken out and stained for further experiments after 7 and 14 days.[18,55]

Tetramer staining and flow cytometry analysis

The cells were resuspended in PBS with human Fc receptor blocking reagent and incubated for 15 min at room temperature prior to tetramer labeling. After that, cells were pelleted and stained for 15 min at room temperature with tetramer (MBL) diluted 1:20 in FACS buffer, followed by 30 min at 4°C for surface staining.[56] Data were collected using an ACEA NovoCyte cytometer and analyses were performed using NovoExpress software.

Mitochondrial-specific dye staining

Different protein-treated cells were stained for 25 min at 37°C in a humid environment containing 5% CO_2 with MitoTracker dyes (MtT) at a concentration of 50 nM.[57] Cells were examined on an ACEA NovoCyte cytometer after being washed twice with PBS.

In vitro T cell functional studies

Target cells were incubated in 20 μg/mL Calcein AM (Dojindo) for 30 min at 37°C to conduct killing experiments. Target cells were either left unpulsed or pulsed for 2 h at 37°C with 25 μg/mL of the peptide (CMV_{PP65}, NLVPMVATV; EBV, GLCTLVAML). Target cells (5×10^3) were cultivated with enlarged effector cells at effector-to-target ratios of 0.1, 1, 5, or 10 for 4 h, Cells were pelleted, and a plate reader was used to measure the fluorescence intensity of supernatant samples.[58] According to the manufacturer's instructions, IFN-γ concentrations in supernatant samples were measured using ELISA (Thermo Fisher, 88-7316).

Intracellular cytokine staining

A total of 2×10^5 human PBMCs, previously expanded with fusion proteins, underwent stimulation by T2 cells in the presence of Brefeldin A and monensin (Thermo Fisher, 00-4980-03) for 16 h at 37°C. During this stimulation, fluorescently labeled anti-CD107a antibodies were added at the initiation of the process. In our experiments, we used the PMA^+ ion as a positive control (the PMA^+ ion is a T cell activator) and PMA, which is a protein kinase C (PKC) activator.[59] Ion (ionomycin) can increase the calcium influx, which results in cytokine production. Treatment with the PMA^+ ion in T cells can increase the PKC-Ras signaling pathway, resulting in cell activations. The cells were plated in a 24-well microtiter plate and stimulated at a ratio of 10:1 with T2 cells. These T2 cells were either unpulsed or had been pulsed with 25 μg/mL of CMV_{PP65} (NLVPMVATV) or EBV (GLCTLVAML) peptides for 2 h at 37°C and subsequently washed twice. To prepare the cells for analysis, the FoxP3/Transcription Factor Staining Buffer Set (Thermo Fisher, 00-5523-00) was used to fix and permeabilize them. This step followed the rinsing of the cells with PBS and staining with antibodies specific to phenotypic markers. Subsequently, the cells were washed and underwent a 30-min staining at room temperature with antibodies targeting intracellular cytokines or proteins before being examined.[19] For *ex vivo* intracellular cytokine staining, spleen cells from OT-1 mice treated with mAPC-mimic were stimulated by B16F10-OVA cells for 16 h. The cells were then processed in a similar manner as described above. Data were collected using an ACEA NovoCyte cytometer and analyses were performed using NovoExpress software.

Single-cell 5′ and V(D)J sequencing

PBMCs from healthy donors were *in vitro* grown for 14 days using fusion proteins and media. Expanded cells were collected, labeled with an antibody, and sorted using magnetic beads for $CD8^+$ T cells. For sequencing and analysis, all of the samples were transported to Personal Biotechnology Co., Ltd. (Shanghai, China). In a nutshell, single-cell 5′ and V(D)J libraries were created using the 10× genomes Chromium Single Cell Immune Profiling Solution technique according to the manufacturer's protocols (10x Genomics V(D)J + 5′ gene expression). Then single-cell 5′ and V(D)J libraries were sequenced by the Illumina Novaseq 6000 using 150 paired-end reads.

scRNA-seq data analysis

The raw sequencing data were processed by the Cell Ranger pipeline (v.7.1, 10x Genomics), which was used to map reads to the reference genome (GRCh38 human) and acquire gene counts to generate expression matrix files for subsequent analysis.[60] We used R package Seurat (v.4.1.1) to filter data and cells were filtered by gene counts more than 5000 or less than 400 and remove the cells with over 10% mitochondrial content.[31] DoubletFinder (v.2.0.3) was used to

remove doublet cells.[61] After filtering, the functions from Seurat (v.4.1.1) was used for dimension-reduction and clustering. Then we used the LogNormalize method of the "Normalization" function to normalize and scale all gene expression. The top 10 dimensions resulted from the principal-component analysis were used for the UMAP or t-SNE.[60] To identify marker genes, we based on Wilcox algorithm, analysis the differential expression of cells in cluster and in other clusters. Because inconsistency and ambiguity remained with the automatic assignment, we then refined the cell cluster annotations based on the expression of canonical marker genes. To investigate the potential functions of differentially expressed genes (DEGs),[62] the Gene Ontology analysis was used with the "clusterProfiler" R package,[35] GSEA was performed on DEGs and the hallmark gene sets were used as the database, absolute value of the normalized enrichment score with p value less than 0.05 were considered as significantly enriched.[63]

scTCR-seq data analysis

The scTCR-seq data were assembled by the Cell Ranger VDJ pipeline (v.7.1, 10x Genomics), and raw FASTQ reads were mapped to the human GRCh38 V(D)J reference genome. Only cells with productive and paired chains were preserved. The cell with the higher UMI count was chosen when more than one consensus sequence for the same chain type was found in a cell.[64] The average read depth per cell for sequencing was 11,178. The downstream analysis that comprises high-confident contigs was conducted using the filtered contig annotation file. The scRepertoire R package (v.0.99.3)[65] was used for TCR analysis, and the clonotype was assigned to the integrated Seurat object as the result of the combination of the VDJ gene components and the nucleotide sequences for the TCRA and TCRB chains. We downsampled an approximately similar number of cells obtained from Blank group and APC-mimic group for clonotype analysis. We discovered 2,777 distinct clonotypes in the Blank group and 625 distinct clonotypes in the APC-mimic group after normalizing the cell counts. A clonotype shared by at least three cells within an individual sample was defined as clonotype expansion, and a clonotype detected in any two or more T cell subtypes within an individual sample was defined as clonotype sharing.

Adoptive cell transfer immunotherapy in an immunodeficient mouse model

NCG mice were subcutaneously injected with 1.5 million K562-CMV cells; 7 days later, mice were randomly assigned and given intravenous injections of 6 million 14-day APC-mimic, pHLA scaffold, or medium expanded PBMCs. An impartial researcher double-blindly measured the tumor area every 2 or 3 days, calculating it as length and width. At the end of the study, mice with tumors larger than 400 mm^2 were euthanized.

In vivo potency assessment and anti-tumor therapy

C57BL/6 mice were subcutaneously injected with 0.8 million B16F10-OVA cells, mice bearing established tumors with area around 20–30 mm^2 (day 6 post inoculation or as indicated) were treated with adoptive transfer of OT-I T cells (5×10^6), followed by i.v. administration of mAPC-mimic (300 μg) or PBS control every other day (or as indicated) starting from day 6 (six doses in total as indicated).[66] Tumor area and body weight were measured every other day. Tumor area was calculated by the formula, area = length × width, from caliper measurements of two orthogonal diameters.

Analyses of tumor-infiltrating immune cells

NCG mice were subcutaneously injected with 1.5 million K562-CMV tumor cells and then underwent i.v. adoptive transfer of 6 million APC-mimic, pHLA scaffold, medium expanded PBMCs on day 7 after tumor inoculation. On day 14, tumors were dissected from the surrounding tissues, weighed, mechanically minced, and stirred at 220 rpm in RPMI 1640 medium with collagenase type IV (1 mg/mL, Gibco/Thermo Fisher Scientific), dispase II (100 μg/mL, Sigma-Aldrich), hyalurondase (100 μg/mL, Sigma-Aldrich), and DNase I (100 μg/mL, Sigma-Aldrich) at 37°C for 60 min for digestion. The digested tumor samples were subjected to ACK lysing buffer for RBC lysis. After being purified by density gradient centrifugation against Ficoll (GE Healthcare), tumor-infiltrating leukocytes were subsequently resuspended in PBS with BSA albumin.[67] Cells were collected in U-bottom 96-well plates for surface marker labeling, blocked with human Fc receptor blocking reagent (MBL), and then treated with the appropriate antibodies at 4°C for 20 min. Live/dead staining was then performed using Zombie Aqua Fixable Dye (BioLegend). The cells were then resuspended in the same buffer for flow cytometry studies after being washed with PBS-containing BSA (0.2%, w/v) in it.

Biochemical indication measurement

Adoptive cell transfer immunotherapy was described above: on day 21, mice were put to death, and serum samples were taken for examination. Stanbio Chemistry Reagents were used to assess the levels of alanine transaminase, aspartate transaminase, creatinine, and blood urea nitrogen in serum[68] in accordance with the manufacturer's recommendations.

ELISpot

The manufacturer's instructions for a commercial kit for the detection of Mouse IFN-γ (Dakewe, cat. DKW22-2000-096) were followed to perform a 24-h ELISpot experiment. In brief, cells were plated in duplicate (0.1 million/100 μL per well), stimulated with phytohemagglutinin (positive control) and OVA peptides (Bankpeptide Technologies) at a final concentration of 4 μg/mL, or medium alone (negative control), and then incubated at 37°C in a humidified atmosphere of 5% CO_2 for 24 h. Plates were washed and then treated with a biotinylated IFN-γ detection antibody for an overnight period at 4°C. After washing the plates, a streptavidin-alkaline phosphatase conjugate was added, and the plates were then incubated for 1 h at 37°C with 5% CO_2. The AEC solution was then poured onto the plates and left on for 20 min at room temperature. Then, wells were scrubbed repeatedly under running water and allowed to air dry overnight. An automated ELISpot reading device (Immunospot Analyzer) was used to count the spots.

Statistical analyses

Statistical analyses were conducted utilizing GraphPad Prism 9 software developed by GraphPad Software. Data are presented as mean ± SEM unless otherwise indicated. For the comparison of two groups, a two-tailed unpaired Student's t test was employed. To assess variations among multiple groups, either a one-way or two-way ANOVA was conducted, followed by Tukey's multiple comparisons test. Survival data were subjected to analysis utilizing the log rank test. Statistically significant differences were not considered when the p values exceeded 0.05.

DATA AND CODE AVAILABILITY

The authors declare that the data supporting the findings of this study are available within the main manuscript and the supplementary figures.

SUPPLEMENTAL INFORMATION

Supplemental information can be found online at https://doi.org/10.1016/j.omton.2024.200827.

ACKNOWLEDGMENTS

This study was supported by Joint Funds of the National Natural Science Foundation of China (grant no. U20A20409) (to S.-Q.C. and L.-Q.P.), the National Natural Science Foundation of China (grant no. 82073750) (to L.-Q.P.), the State Key Laboratory for Diagnosis and Treatment of Infectious Diseases Funding (grant no. zz202303) (to L.-Q.P.), the National Key Research and Development Program of China (grant no. 2023YFC3403900) (to L.-Q.P.), the Fundamental Research Funds for the Central Universities (no. 2020QNA7005) (to L.-Q.P.), and Zhejiang Province "Qianjiang Talent Plan" (to L.-Q.P.).

AUTHOR CONTRIBUTIONS

L.-Q.P. and S.-Q.C. conceived and directed the project. Y.W., X.L., Y.-P.S., J.-T.N., Y.-K.D., S.-J.J., and Y.-C.X. performed all experiments. Y.W. analyzed data. L.-Q.P. and Y.W. wrote and revised the paper. All authors contributed to discussions.

DECLARATION OF INTERESTS

The authors have filed a patent (granted, patent number: 2022108197741) on the APC-mimic sequence, design, and its application.

REFERENCES

1. Lenschow, D.J., Walunas, T.L., and Bluestone, J.A. (1996). CD28/B7 system of T cell costimulation. Annu. Rev. Immunol. *14*, 233–258. https://doi.org/10.1146/annurev.immunol.14.1.233.

2. Gill, J., and Prasad, V. (2019). A reality check of the accelerated approval of immune-checkpoint inhibitors. Nat. Rev. Clin. Oncol. *16*, 656–658. https://doi.org/10.1038/s41571-019-0260-y.

3. Tang, J., Yu, J.X., Hubbard-Lucey, V.M., Neftelinov, S.T., Hodge, J.P., and Lin, Y. (2018). Trial watch: The clinical trial landscape for PD1/PDL1 immune checkpoint inhibitors. Nat. Rev. Drug Discov. *17*, 854–855. https://doi.org/10.1038/nrd.2018.210.

4. Sobhani, N., Tardiel-Cyril, D.R., Davtyan, A., Generali, D., Roudi, R., and Li, Y. (2021). CTLA-4 in Regulatory T Cells for Cancer Immunotherapy. Cancers *13*, 1440. https://doi.org/10.3390/cancers13061440.

5. Haslam, A., and Prasad, V. (2019). Estimation of the Percentage of US Patients With Cancer Who Are Eligible for and Respond to Checkpoint Inhibitor Immunotherapy Drugs. JAMA Netw. Open *2*, e192535. https://doi.org/10.1001/jamanetworkopen.2019.2535.

6. Brahmer, J.R., Lacchetti, C., Schneider, B.J., Atkins, M.B., Brassil, K.J., Caterino, J.M., Chau, I., Ernstoff, M.S., Gardner, J.M., Ginex, P., et al. (2018). Management of Immune-Related Adverse Events in Patients Treated With Immune Checkpoint Inhibitor Therapy: American Society of Clinical Oncology Clinical Practice Guideline. J. Clin. Oncol. *36*, 1714–1768. https://doi.org/10.1200/JCO.2017.77.6385.

7. Puzanov, I., Diab, A., Abdallah, K., Bingham, C.O., Brogdon, C., Dadu, R., Hamad, L., Kim, S., Lacouture, M.E., LeBoeuf, N.R., et al. (2017). Managing toxicities associated with immune checkpoint inhibitors: consensus recommendations from the Society for Immunotherapy of Cancer (SITC) Toxicity Management Working Group. J. Immunother. Cancer *5*, 95. https://doi.org/10.1186/s40425-017-0300-z.

8. June, C.H., O'Connor, R.S., Kawalekar, O.U., Ghassemi, S., and Milone, M.C. (2018). CAR T cell immunotherapy for human cancer. Science *359*, 1361–1365. https://doi.org/10.1126/science.aar6711.

9. Sadelain, M., Brentjens, R., and Rivière, I. (2013). The Basic Principles of Chimeric Antigen Receptor Design. Cancer Discov. *3*, 388–398. https://doi.org/10.1158/2159-8290.CD-12-0548.

10. Neelapu, S.S., Locke, F.L., Bartlett, N.L., Lekakis, L.J., Miklos, D.B., Jacobson, C.A., Braunschweig, I., Oluwole, O.O., Siddiqi, T., Lin, Y., et al. (2017). Axicabtagene Ciloleucel CAR T-Cell Therapy in Refractory Large B-Cell Lymphoma. N. Engl. J. Med. *377*, 2531–2544. https://doi.org/10.1056/NEJMoa1707447.

11. Sterner, R.C., and Sterner, R.M. (2021). CAR-T cell therapy: current limitations and potential strategies. Blood Cancer J. *11*, 69. https://doi.org/10.1038/s41408-021-00459-7.

12. Kim, J.V., Latouche, J.-B., Rivière, I., and Sadelain, M. (2004). The ABCs of artificial antigen presentation. Nat. Biotechnol. *22*, 403–410. https://doi.org/10.1038/nbt955.

13. Jiang, Y., Krishnan, N., Zhou, J., Chekuri, S., Wei, X., Kroll, A.V., Yu, C.L., Duan, Y., Gao, W., Fang, R.H., and Zhang, L. (2020). Engineered Cell-Membrane-Coated Nanoparticles Directly Present Tumor Antigens to Promote Anticancer Immunity. Adv. Mater. *32*, 2001808. https://doi.org/10.1002/adma.202001808.

14. Maus, M.V., Thomas, A.K., Leonard, D.G.B., Allman, D., Addya, K., Schlienger, K., Riley, J.L., and June, C.H. (2002). Ex vivo expansion of polyclonal and antigen-specific cytotoxic T lymphocytes by artificial APCs expressing ligands for the T-cell receptor, CD28 and 4-1BB. Nat. Biotechnol. *20*, 143–148. https://doi.org/10.1038/nbt0202-143.

15. Tham, E.L., Jensen, P.L., and Mescher, M.F. (2001). Activation of antigen-specific T cells by artificial cell constructs having immobilized multimeric peptide–class I complexes and recombinant B7–Fc proteins. J. Immunol. Methods *249*, 111–119. https://doi.org/10.1016/S0022-1759(00)00335-5.

16. Singha, S., Shao, K., Yang, Y., Clemente-Casares, X., Solé, P., Clemente, A., Blanco, J., Dai, Q., Song, F., Liu, S.W., et al. (2017). Peptide–MHC-based nanomedicines for autoimmunity function as T-cell receptor microclustering devices. Nat. Nanotechnol. *12*, 701–710. https://doi.org/10.1038/nnano.2017.56.

17. Ichikawa, J., Yoshida, T., Isser, A., Laino, A.S., Vassallo, M., Woods, D., Kim, S., Oelke, M., Jones, K., Schneck, J.P., and Weber, J.S. (2020). Rapid Expansion of Highly Functional Antigen-Specific T Cells from Patients with Melanoma by Nanoscale Artificial Antigen-Presenting Cells. Clin. Cancer Res. *26*, 3384–3396. https://doi.org/10.1158/1078-0432.CCR-19-3487.

18. Cheung, A.S., Zhang, D.K.Y., Koshy, S.T., and Mooney, D.J. (2018). Scaffolds that mimic antigen-presenting cells enable ex vivo expansion of primary T cells. Nat. Biotechnol. *36*, 160–169. https://doi.org/10.1038/nbt.4047.

19. Li, M., Garforth, S.J., O'Connor, K.E., Su, H., Lee, D.M., Celikgil, A., Chaparro, R.J., Seidel, R.D., Jones, R.B., Arav-Boger, R., et al. (2021). T cell receptor–targeted immunotherapeutics drive selective *in vivo* HIV- and CMV-specific T cell expansion in humanized mice. J. Clin. Invest. *131*, e141051. https://doi.org/10.1172/JCI141051.

20. Ridgway, J.B., Presta, L.G., and Carter, P. (1996). "Knobs-into-holes" engineering of antibody CH3 domains for heavy chain heterodimerization. Protein Eng. *9*, 617–621. https://doi.org/10.1093/protein/9.7.617.

21. Serra, P., Garabatos, N., Singha, S., Fandos, C., Garnica, J., Solé, P., Parras, D., Yamanouchi, J., Blanco, J., Tort, M., et al. (2019). Increased yields and biological

potency of knob-into-hole-based soluble MHC class II molecules. Nat. Commun. *10*, 4917. https://doi.org/10.1038/s41467-019-12902-2.

22. Liu, P., Gao, X., Lundin, V., Shi, C., Adem, Y., Lin, K., Jiang, G., Kao, Y.-H., Yang, F., Michels, D., et al. (2020). Probing the Impact of the Knob-into-Hole Mutations on the Structure and Function of a Therapeutic Antibody. Anal. Chem. *92*, 1582–1588. https://doi.org/10.1021/acs.analchem.9b04855.

23. Hezareh, M., Hessell, A.J., Jensen, R.C., van de Winkel, J.G., and Parren, P.W. (2001). Effector Function Activities of a Panel of Mutants of a Broadly Neutralizing Antibody against Human Immunodeficiency Virus Type 1. J. Virol. *75*, 12161–12168. https://doi.org/10.1128/jvi.75.24.12161-12168.2001.

24. Schlothauer, T., Herter, S., Koller, C.F., Grau-Richards, S., Steinhart, V., Spick, C., Kubbies, M., Klein, C., Umaña, P., and Mössner, E. (2016). Novel human IgG1 and IgG4 Fc-engineered antibodies with completely abolished immune effector functions. Protein Eng. Des. Sel. *29*, 457–466. https://doi.org/10.1093/protein/gzw040.

25. Vafa, O., Gilliland, G.L., Brezski, R.J., Strake, B., Wilkinson, T., Lacy, E.R., Scallon, B., Teplyakov, A., Malia, T.J., and Strohl, W.R. (2014). An engineered Fc variant of an IgG eliminates all immune effector functions via structural perturbations. Methods *65*, 114–126. https://doi.org/10.1016/j.ymeth.2013.06.035.

26. Mori, M., Beatty, P.G., Graves, M., Boucher, K.M., and Milford, E.L. (1997). HLA gene and haplotype frequencies in the North American population: the National Marrow Donor Program Donor Registry. Transplantation *64*, 1017–1027. https://doi.org/10.1097/00007890-199710150-00014.

27. Miller, B.C., Sen, D.R., Al Abosy, R., Bi, K., Virkud, Y.V., LaFleur, M.W., Yates, K.B., Lako, A., Felt, K., Naik, G.S., et al. (2019). Subsets of exhausted CD8+ T cells differentially mediate tumor control and respond to checkpoint blockade. Nat. Immunol. *20*, 326–336. https://doi.org/10.1038/s41590-019-0312-6.

28. LaFleur, M.W., Nguyen, T.H., Coxe, M.A., Miller, B.C., Yates, K.B., Gillis, J.E., Sen, D.R., Gaudiano, E.F., Al Abosy, R., Freeman, G.J., et al. (2019). PTPN2 regulates the generation of exhausted CD8+ T cell subpopulations and restrains tumor immunity. Nat. Immunol. *20*, 1335–1347. https://doi.org/10.1038/s41590-019-0480-4.

29. Han, J., Khatwani, N., Searles, T.G., Turk, M.J., and Angeles, C.V. (2020). Memory CD8+ T cell responses to cancer. Semin. Immunol. *49*, 101435. https://doi.org/10.1016/j.smim.2020.101435.

30. Henning, A.N., Roychoudhuri, R., and Restifo, N.P. (2018). Epigenetic control of CD8+ T cell differentiation. Nat. Rev. Immunol. *18*, 340–356. https://doi.org/10.1038/nri.2017.146.

31. Butler, A., Hoffman, P., Smibert, P., Papalexi, E., and Satija, R. (2018). Integrating single-cell transcriptomic data across different conditions, technologies, and species. Nat. Biotechnol. *36*, 411–420. https://doi.org/10.1038/nbt.4096.

32. Stuart, T., Butler, A., Hoffman, P., Hafemeister, C., Papalexi, E., Mauck, W.M., Hao, Y., Stoeckius, M., Smibert, P., and Satija, R. (2019). Comprehensive Integration of Single-Cell Data. Cell *177*, 1888–1902.e21. https://doi.org/10.1016/j.cell.2019.05.031.

33. Schmiedel, B.J., Singh, D., Madrigal, A., Valdovino-Gonzalez, A.G., White, B.M., Zapardiel-Gonzalo, J., Ha, B., Altay, G., Greenbaum, J.A., McVicker, G., et al. (2018). Impact of Genetic Polymorphisms on Human Immune Cell Gene Expression. Cell *175*, 1701–1715.e16. https://doi.org/10.1016/j.cell.2018.10.022.

34. Monaco, G., Lee, B., Xu, W., Mustafah, S., Hwang, Y.Y., Carré, C., Burdin, N., Visan, L., Ceccarelli, M., Poidinger, M., et al. (2019). RNA-Seq Signatures Normalized by mRNA Abundance Allow Absolute Deconvolution of Human Immune Cell Types. Cell Rep. *26*, 1627–1640.e7. https://doi.org/10.1016/j.celrep.2019.01.041.

35. Alexa, A., Rahnenführer, J., and Lengauer, T. (2006). Improved scoring of functional groups from gene expression data by decorrelating GO graph structure. Bioinf. Oxf. Engl. *22*, 1600–1607. https://doi.org/10.1093/bioinformatics/btl140.

36. Giudice, V., Feng, X., Lin, Z., Hu, W., Zhang, F., Qiao, W., Ibanez, M.D.P.F., Rios, O., and Young, N.S. (2018). Deep sequencing and flow cytometric characterization of expanded effector memory CD8+CD57+ T cells frequently reveals T-cell receptor Vβ oligoclonality and CDR3 homology in acquired aplastic anemia. Haematologica *103*, 759–769. https://doi.org/10.3324/haematol.2017.176701.

37. Bentzen, A.K., and Hadrup, S.R. (2019). T-cell-receptor cross-recognition and strategies to select safe T-cell receptors for clinical translation. Immunooncol. Technol. *2*, 1–10. https://doi.org/10.1016/j.iotech.2019.06.003.

38. Schmittnaegel, M., Hoffmann, E., Imhof-Jung, S., Fischer, C., Drabner, G., Georges, G., Klein, C., and Knoetgen, H. (2016). A New Class of Bifunctional Major Histocompatibility Class I Antibody Fusion Molecules to Redirect CD8 T Cells. Mol. Cancer Ther. *15*, 2130–2142. https://doi.org/10.1158/1535-7163.MCT-16-0207.

39. Suntharalingam, G., Perry, M.R., Ward, S., Brett, S.J., Castello-Cortes, A., Brunner, M.D., and Panoskaltsis, N. (2006). Cytokine storm in a phase 1 trial of the anti-CD28 monoclonal antibody TGN1412. N. Engl. J. Med. *355*, 1018–1028. https://doi.org/10.1056/NEJMoa063842.

40. Hansel, T.T., Kropshofer, H., Singer, T., Mitchell, J.A., and George, A.J.T. (2010). The safety and side effects of monoclonal antibodies. Nat. Rev. Drug Discov. *9*, 325–338. https://doi.org/10.1038/nrd3003.

41. Linsley, P.S., Greene, J.L., Brady, W., Bajorath, J., Ledbetter, J.A., and Peach, R. (1994). Human B7-1 (CD80) and B7-2 (CD86) bind with similar avidities but distinct kinetics to CD28 and CTLA-4 receptors. Immunity *1*, 793–801. https://doi.org/10.1016/S1074-7613(94)80021-9.

42. Collins, A.V., Brodie, D.W., Gilbert, R.J.C., Iaboni, A., Manso-Sancho, R., Walse, B., Stuart, D.I., van der Merwe, P.A., and Davis, S.J. (2002). The interaction properties of costimulatory molecules revisited. Immunity *17*, 201–210. https://doi.org/10.1016/s1074-7613(02)00362-x.

43. Sugiura, D., Maruhashi, T., Okazaki, I.M., Shimizu, K., Maeda, T.K., Takemoto, T., and Okazaki, T. (2019). Restriction of PD-1 function by *cis* -PD-L1/CD80 interactions is required for optimal T cell responses. Science *364*, 558–566. https://doi.org/10.1126/science.aav7062.

44. Zhao, Y., Lee, C.K., Lin, C.-H., Gassen, R.B., Xu, X., Huang, Z., Xiao, C., Bonorino, C., Lu, L.-F., Bui, J.D., and Hui, E. (2019). PD-L1:CD80 Cis-Heterodimer Triggers the Co-stimulatory Receptor CD28 While Repressing the Inhibitory PD-1 and CTLA-4 Pathways. Immunity *51*, 1059–1073.e9. https://doi.org/10.1016/j.immuni.2019.11.003.

45. Miyama, T., Kawase, T., Kitaura, K., Chishaki, R., Shibata, M., Oshima, K., Hamana, H., Kishi, H., Muraguchi, A., Kuzushima, K., et al. (2017). Highly functional T-cell receptor repertoires are abundant in stem memory T cells and highly shared among individuals. Sci. Rep. *7*, 3663. https://doi.org/10.1038/s41598-017-03855-x.

46. Elhanati, Y., Sethna, Z., Callan, C.G., Mora, T., and Walczak, A.M. (2018). Predicting the spectrum of TCR repertoire sharing with a data-driven model of recombination. Immunol. Rev. *284*, 167–179. https://doi.org/10.1111/imr.12665.

47. Baker, B.M., Scott, D.R., Blevins, S.J., and Hawse, W.F. (2012). Structural and dynamic control of T-cell receptor specificity, cross-reactivity, and binding mechanism. Immunol. Rev. *250*, 10–31. https://doi.org/10.1111/j.1600-065X.2012.01165.x.

48. Smith-Garvin, J.E., Koretzky, G.A., and Jordan, M.S. (2009). T cell activation. Annu. Rev. Immunol. *27*, 591–619. https://doi.org/10.1146/annurev.immunol.021908.132706.

49. Oliveira, G., and Wu, C.J. (2023). Dynamics and specificities of T cells in cancer immunotherapy. Nat. Rev. Cancer *23*, 295–316. https://doi.org/10.1038/s41568-023-00560-y.

50. Lang, F., Schrörs, B., Löwer, M., Türeci, Ö., and Sahin, U. (2022). Identification of neoantigens for individualized therapeutic cancer vaccines. Nat. Rev. Drug Discov. *21*, 261–282. https://doi.org/10.1038/s41573-021-00387-y.

51. Sahin, U., Derhovanessian, E., Miller, M., Kloke, B.-P., Simon, P., Löwer, M., Bukur, V., Tadmor, A.D., Luxemburger, U., Schrörs, B., et al. (2017). Personalized RNA mutanome vaccines mobilize poly-specific therapeutic immunity against cancer. Nature *547*, 222–226. https://doi.org/10.1038/nature23003.

52. Portolano, N., Watson, P.J., Fairall, L., Millard, C.J., Milano, C.P., Song, Y., Cowley, S.M., and Schwabe, J.W.R. (2014). Recombinant protein expression for structural biology in HEK 293F suspension cells: a novel and accessible approach. J. Vis. Exp. e51897. https://doi.org/10.3791/51897.

53. Heyduk, E., Hickey, R., Pozzi, N., and Heyduk, T. (2018). Peptide ligand-based ELISA reagents for antibody detection. Anal. Biochem. *559*, 55–61. https://doi.org/10.1016/j.ab.2018.08.012.

54. Li, W., Gao, T., Lou, C., Wang, H., Liu, Y., and Cao, A. (2022). Biotinylated Au Nanoparticle-Based Artificial Antibody for Detection of Lysozyme by the Lateral Flow Immunoassay and Enzyme-Linked Immunosorbent Assay. ACS Appl. Nano Mater. *5*, 12571–12581. https://doi.org/10.1021/acsanm.2c02268.

55. Zhang, D.K.Y., Cheung, A.S., and Mooney, D.J. (2020). Activation and expansion of human T cells using artificial antigen-presenting cell scaffolds. Nat. Protoc. *15*, 773–798. https://doi.org/10.1038/s41596-019-0249-0.

56. Liu, G., Chen, H., Cao, X., Jia, L., Rui, W., Zheng, H., Huang, D., Liu, F., Liu, Y., Zhao, X., et al. (2022). Efficacy of pp65-specific TCR-T cell therapy in treating cytomegalovirus infection after hematopoietic stem cell transplantation. Am. J. Hematol. *97*, 1453–1463. https://doi.org/10.1002/ajh.26708.

57. Wang, X., Su, B., Siedlak, S.L., Moreira, P.I., Fujioka, H., Wang, Y., Casadesus, G., and Zhu, X. (2008). Amyloid-beta overproduction causes abnormal mitochondrial dynamics via differential modulation of mitochondrial fission/fusion proteins. Proc. Natl. Acad. Sci. USA *105*, 19318–19323. https://doi.org/10.1073/pnas.0804871105.

58. Quayle, S.N., Girgis, N., Thapa, D.R., Merazga, Z., Kemp, M.M., Histed, A., Zhao, F., Moreta, M., Ruthardt, P., Hulot, S., et al. (2020). CUE-101, a Novel E7-pHLA-IL2-Fc Fusion Protein, Enhances Tumor Antigen-Specific T-Cell Activation for the Treatment of HPV16-Driven Malignancies. Clin. Cancer Res. *26*, 1953–1964. https://doi.org/10.1158/1078-0432.CCR-19-3354.

59. Downward, J., Graves, J.D., Warne, P.H., Rayter, S., and Cantrell, D.A. (1990). Stimulation of p21ras upon T-cell activation. Nature *346*, 719–723. https://doi.org/10.1038/346719a0.

60. Azizi, E., Carr, A.J., Plitas, G., Cornish, A.E., Konopacki, C., Prabhakaran, S., Nainys, J., Wu, K., Kiseliovas, V., Setty, M., et al. (2018). Single-Cell Map of Diverse Immune Phenotypes in the Breast Tumor Microenvironment. Cell *174*, 1293–1308.e36. https://doi.org/10.1016/j.cell.2018.05.060.

61. McGinnis, C.S., Murrow, L.M., and Gartner, Z.J. (2019). DoubletFinder: Doublet Detection in Single-Cell RNA Sequencing Data Using Artificial Nearest Neighbors. Cell Syst. *8*, 329–337.e4. https://doi.org/10.1016/j.cels.2019.03.003.

62. Vandenbon, A., and Diez, D. (2020). A clustering-independent method for finding differentially expressed genes in single-cell transcriptome data. Nat. Commun. *11*, 4318. https://doi.org/10.1038/s41467-020-17900-3.

63. Subramanian, A., Tamayo, P., Mootha, V.K., Mukherjee, S., Ebert, B.L., Gillette, M.A., Paulovich, A., Pomeroy, S.L., Golub, T.R., Lander, E.S., and Mesirov, J.P. (2005). Gene set enrichment analysis: a knowledge-based approach for interpreting genome-wide expression profiles. Proc. Natl. Acad. Sci. USA *102*, 15545–15550. https://doi.org/10.1073/pnas.0506580102.

64. Gao, S., Wu, Z., Arnold, B., Diamond, C., Batchu, S., Giudice, V., Alemu, L., Raffo, D.Q., Feng, X., Kajigaya, S., et al. (2022). Single-cell RNA sequencing coupled to TCR profiling of large granular lymphocyte leukemia T cells. Nat. Commun. *13*, 1982. https://doi.org/10.1038/s41467-022-29175-x.

65. Borcherding, N., Bormann, N.L., and Kraus, G. (2020). scRepertoire: An R-based toolkit for single-cell immune receptor analysis. F1000Res. *9*, 47. https://doi.org/10.12688/f1000research.22139.2.

66. Zhang, X., Luo, M., Dastagir, S.R., Nixon, M., Khamhoung, A., Schmidt, A., Lee, A., Subbiah, N., McLaughlin, D.C., Moore, C.L., et al. (2021). Engineered red blood cells as an off-the-shelf allogeneic anti-tumor therapeutic. Nat. Commun. *12*, 2637. https://doi.org/10.1038/s41467-021-22898-3.

67. Guo, Y., Xie, Y.-Q., Gao, M., Zhao, Y., Franco, F., Wenes, M., Siddiqui, I., Bevilacqua, A., Wang, H., Yang, H., et al. (2021). Metabolic reprogramming of terminally exhausted CD8+ T cells by IL-10 enhances anti-tumor immunity. Nat. Immunol. *22*, 746–756. https://doi.org/10.1038/s41590-021-00940-2.

68. Ren, H., Yong, J., Yang, Q., Yang, Z., Liu, Z., Xu, Y., Wang, H., Jiang, X., Miao, W., and Li, X. (2021). Self-assembled FeS-based cascade bioreactor with enhanced tumor penetration and synergistic treatments to trigger robust cancer immunotherapy. Acta Pharm. Sin. B *11*, 3244–3261. https://doi.org/10.1016/j.apsb.2021.05.005.